

The Thermal State of 18–24 Ma Upper Lithosphere Subducting Below the Nicoya Peninsula, Northern Costa Rica Margin

M. Hutnak, A. T. Fisher, C. A. Stein, R. Harris, K. Wang, E. Silver, G. Spinelli, M. Pfender, H. Villinger, R. MacKnight, P. Costa Pisani, H. DeShon, and C. Diamente

Abstract

Early studies of the thermal state of the Cocos plate subducting beneath the northern Costa Rica margin identified two adjacent areas of higher (>100 mW/m²) and lower (<30 mW/m²) heat flow. Measurements on crust formed at the Cocos-Nazca spreading center (CNS) were generally in agreement with later predictions from conductive lithospheric cooling models, whereas measurements on East Pacific Rise (EPR) crust were commonly lower by $\sim 70\%$. However, the sparse distribution of early data precluded confident determination of the cause(s) for the heat-flow deficit on EPR-generated seafloor, nor did they allow an assessment of the nature of the transition between warmer and cooler regions. We present new thermal, swath map, and seismic data collected on the incoming plate offshore of Costa Rica, seaward of the Middle America Trench (MAT), in an area containing several tectonic boundaries, including the plate suture between EPR- and CNS-generated seafloor. We find that most transitions from warm to anomalously cool thermal conditions are not directly associated with any of the tectonic boundaries and that vigorous local hydrothermal circulation in uppermost basement is responsible for low heat-flow values on the cooler part of the plate. Thermal data in the vicinity of Ocean Drilling Program (ODP) Site 1039, located within the trench, indicate that the drill site is surrounded on three sides by regions of warmer seafloor. Heat-flow data across normal faults outboard of the MAT suggest that these faults do not allow vertical advective extraction of lithospheric heat in this location. Satellite and hydrosweep data show that seamounts are common features on EPR-generated seafloor, whereas CNS-generated seafloor immediately adjacent to the plate suture and the MAT is devoid of seamounts. It appears that most of the EPR-generated crust in this area is cooled on a regional basis by hydrothermal fluids recharging and discharging through seamounts

and other basement outcrops. Analytical model calculations suggest that the vertical extent of hydrothermal cooling may be limited to the upper 100–600 m of basement, and effective upper-basement permeabilities are on the order of 10^{-10} – 10^{-8} m².

Introduction

The thermal state of subducting oceanic plates influences melting conditions in the overlying mantle wedge, the extent of sediment dewatering associated with mineralogical and rheological transitions, the occurrence of gas hydrates along the active margin, and the nature of tectonic and seismic processes at depth [e.g., Fisher *et al.*, 2003b; Gaetani and Grove, 1998; Hyndman and Wang, 1993; Ruppel and Kinoshita, 2000; Saffer and Marone, 2003; Stein, 2003; Zhao *et al.*, 1997]. Determining thermal conditions within subduction zones is difficult because drilling to necessary depths poses severe technical challenges, and seafloor thermal data collected on the margin are typically influenced by processes such as fluid flow and frictional heating along faults [e.g., Henry and Wang, 1991; Iwamori, 1998; Peacock and Wang, 1999]. In this paper we examine the thermal state of the upper lithosphere approaching the subduction zone along the Middle America Trench, offshore of the Nicoya Peninsula, Costa Rica. Much recent work in this region has focused on conditions within the upper plate and along the plate boundary within the subduction zone, but there has been relatively little emphasis on the nature of thermal conditions within the incoming plate prior to subduction. Understanding the thermal state of the incoming plate is important because it comprises both boundary and initial conditions for thermal models of subduction processes.

Any rigorous assessment of thermal conditions within oceanic lithosphere should include consideration of hydrothermal circulation. The upper oceanic crust is typically highly permeable, and hosts large-scale flows of water, energy, and solutes [e.g., Schultz and Elderfield, 1997; Sclater *et al.*, 1980]. These fluxes help to maintain the chemistry of the ocean, change the physical and geochemical state of the lithosphere, transport volatiles into the mantle, and support a vast subsurface biosphere [e.g., Alt *et al.*, 1996; Cowen *et al.*, 2003; Elderfield and Schultz, 1996; Jacobson, 1992; Plank and Langmuir, 1993; Wheat *et al.*, 2003].

Although much attention in the past has focused on high-temperature (>300°C) hydrothermal vents at mid-ocean ridge spreading centers, global heat flow data indicate that advective heat loss from ridge flanks is more than 3 times that at the ridge axis [Mottl and Wheat, 1994; Stein and Stein, 1994]. Because this off-axis flux occurs at much lower temperatures (<100°C), the corresponding mass flux of seawater through the crust is inferred to be at least 10–100 times greater than at the ridge axis [Mottl and Wheat, 1994; Schultz and Elderfield, 1997; Stein and Stein, 1994]. Ridge-flank fluxes of some solutes

approach or even exceed those on the ridge crest and from riverine sources [Elderfield and Schultz, 1996; Mottl, 2003]. Advective heat loss from the ocean crust extends, on average, to a global mean age of ~65 Ma, but some regions lose heat advectively to greater ages, and fluid circulation within basement is capable of redistributing heat well beyond 100 Ma [Noel and Hounslow, 1988; Stein and Stein, 1994; Von Herzen, 2004].

In this synthesis, we briefly summarize the tectonic setting (discussed in greater detail elsewhere in this volume) and review early studies of thermal conditions within the lithosphere of the Cocos plate offshore northern Costa Rica. This includes a short discussion of results associated with Ocean Drilling Program (ODP) Leg 170, which examined the margin wedge and trench immediately offshore of the Nicoya Peninsula, and results from a predrilling survey cruise that focused on thermal conditions at planned drilling sites. The main focus of this paper concerns new results from two recent expeditions to this region (comprising the “TicoFlux” program), which sought to elucidate the extent, nature, and causes for differences in thermal conditions within adjacent parts of the Cocos plate prior to subduction.

Regional Setting

Costa Rica lies at the southern end of the Central American island arc system, where the Cocos plate subducts at ~85 mm/yr beneath the Caribbean plate [DeMets, 2001], forming the Middle America Trench (MAT; fig. 4.1). The 18–24 Ma seafloor offshore the Nicoya Peninsula, Costa Rica, has had a complex tectonic history and is commonly considered as comprising several distinct tectonic subregions [e.g., Barckhausen *et al.*, 2001; Meschede *et al.*, 1998; Ranero and von Huene, 2000; von Huene *et al.*, 2000].

Toward the middle of the Nicoya Peninsula, offshore magnetic lineations abruptly switch orientation by roughly 90°, distinguishing seafloor formed at the East Pacific Rise (EPR, trench-parallel isochrons) from that formed at the Cocos-Nazca Spreading Center (CNS, trench-perpendicular isochrons). The boundary between EPR- and CNS-generated seafloor is a combination of a triple junction trace and a fracture zone trace (referred to by Fisher *et al.* [2003b] as a “plate suture”). During earlier studies on a regional scale, the plate suture was called the “rough-smooth boundary (RSB),” a reference to the Cocos Ridge and associated rough topography related to the passing of the Cocos plate over the Galapagos hot spot [Hey, 1977]. Seafloor seaward of the northern segment of the Nicoya Peninsula was noted to be relatively smooth in comparison to that off the southern portion [e.g., von Huene *et al.*, 2000], but as discussed below, previously unidentified seamounts are important thermal (and hydrogeologic) features to the north of the plate suture.

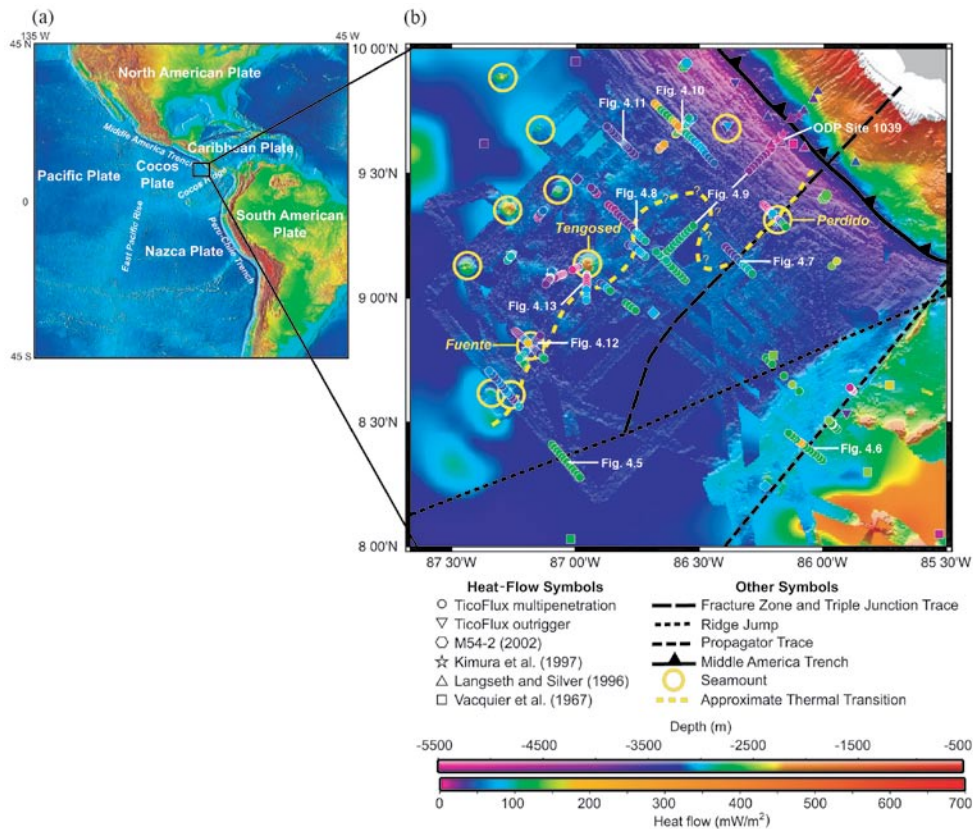


Figure 4.1 (a) Regional map showing tectonic plates, spreading centers, and regional bathymetry. Dark box indicates the TicoFlux study region in figure 4.1b. (Image courtesy NOAA-NGDC: <http://www.ngdc.noaa.gov>). (b) Seafloor bathymetry based on satellite gravimetry and swath mapping [Barckhausen et al., 2001; Fisher et al., 2003b; von Huene et al., 2000], overlain by tectonic boundaries derived from bathymetry, gravity, and magnetics [Barckhausen et al., 2001; Hey, 1977; Meschede et al., 1998]. Color-coded symbols indicate heat-flow values: circles correspond to TicoFlux studies, while other sources are as labeled (M54-2 data courtesy of I. Grevemeyer (personal communication, 2002). ODP Leg 170 drilled a series of holes across the trench and onto the margin wedge northwest of the triple-junction trace [Kimura et al., 1997]. Dashed yellow line indicates approximate thermal transition along seismic transects from anomalously low heat flow to areas with elevated heat flow. EPR-generated crust to the north of the triple junction and fracture zone traces has heat flow suppressed by roughly 70%, whereas CNS-generated crust to the south generally has heat flow that matches conductive lithospheric cooling models. Of note are the prevalence seamounts (gold circles) on EPR-generated crust, which allow recharging and discharging fluids to bypass the 300–500 m thick sediments and allow for the efficient extraction of large amounts of lithospheric heat.

Two additional tectonic boundaries within this part of the Cocos plate are important for the discussion of lithospheric thermal state: traces of a ridge jump and a propagating ridge [Barckhausen *et al.*, 2001; Meschede *et al.*, 1998] (fig. 4.1). The ridge jump helps to define the southern edge of a triangular block of CNS-generated lithosphere adjacent to the plate suture and the MAT and forms part of the boundary between CNS-generated and EPR-generated seafloor. The propagator trace cuts entirely across CNS-generated seafloor and offsets the magnetic anomalies by several tens of kilometers.

The Costa Rica margin is seismically very active, with at least four earthquakes of magnitude >7 having occurred in the last 200 years. A significant change of ~5–10 km in the depth of the updip limit of background microseismicity along the Nicoya Peninsula loosely coincides with the plate suture, suggesting that the thermal state of the crust (colder EPR versus warmer CNS) influences the seismogenic updip limit along the Nicoya portion of the MAT [Newman *et al.*, 2002].

ODP Leg 170 [Kimura *et al.*, 1997] drilled several sites on the subduction wedge offshore of the Nicoya Peninsula, and Site 1039 in the MAT, which has become a de facto reference site for regional studies of stratigraphy and sedimentation history on the incoming plate (fig. 4.1). Drilling at Site 1039 penetrated 180 m of diatom-rich hemipelagic claystone overlying 200 m of nanofossil-rich carbonate ooze, with the oldest recovered sediment dated at 16.5 Ma. The base of the sediment section consisted of brown claystone intruded by gabbroic sills. Frontal accretion of the stratigraphic section does not occur as the plate passes beneath the toe of the margin wedge [Kimura *et al.*, 1997; Silver *et al.*, 2001], although there is seismic evidence for underplating at deeper levels [McIntosh and Sen, 2000].

Thermal Studies Along the Costa Rica Margin

Studies Prior to TicoFlux

The earliest heat-flow data from seaward of the MAT were collected at a time when researchers were trying to understand the most fundamental aspects of heat loss from oceanic lithosphere [e.g., Bullard *et al.*, 1956; Langseth *et al.*, 1965; Vacquier *et al.*, 1967; Von Herzen and Uyeda, 1963] and before the precise age of the seafloor in this area was known [Anderson and Hobart, 1976]. It was thought that relatively high heat-flow values found near the EPR and other mid-ocean ridges might result from convection or heat sources in the mantle, and there was speculation as to the possible occurrence of hydrothermal circulation in these areas of generally high, but scattered, values [e.g., Elder, 1965; Langseth *et al.*, 1966; Lee and Uyeda, 1965]. Because heat-flow technology at the time made each measurement difficult and time consuming, heat-flow

stations on early expeditions tended to be widely separated, with between-measurement spacing commonly being 100 km or more. In addition, the lack of continuous bathymetric maps and the absence of high-quality seismic data prevented a thorough assessment of the geological context of many early measurements, including the influence of buried basement relief and seafloor refraction on heat-flow measurements [e.g., *Sclater et al.*, 1976; *Von Herzen and Uyeda*, 1963].

Early studies of the eastern Pacific Ocean basin were able to clearly identify areas of relatively high (>100 mW/m²) and low (<30 mW/m²) heat flow. Higher values were generally found close to the EPR, but there were also elevated values found near the Cocos Ridge [*Vacquier et al.*, 1967; *Von Herzen and Uyeda*, 1963], which were attributed to recent igneous intrusions. Although elevated heat flow associated with the EPR was generally related to the upwelling limb of a mantle convection cell, there was no corresponding decrease in heat flow with increasing proximity to the MAT, which seemed to preclude the occurrence of mantle downwelling in this region. Low heat-flow values were found in the Guatemala Basin to the north, another observation that could not be attributed to mantle convection, and it was suggested that there might be a relative deficiency in heat producing elements within the mantle in this region.

In fact, the data collected and compiled by *Vacquier et al.* [1967] suggested that there were considerable differences in oceanic heat flow between EPR- and CNS-generated seafloor offshore of the Nicoya Peninsula (fig. 4.1). Conductive lithospheric cooling models suggest that 18–24 Ma seafloor should have heat flow of 95–120 mW/m² [e.g., *Parsons and Sclater*, 1977; *Stein and Stein*, 1992]. Pre-1990s heat-flow data from offshore of the Nicoya Peninsula yielded mean heat flow values of 31 mW/m² on EPR-generated seafloor and 110 mW/m² on CNS-generated seafloor (heat-flow fractions of ~ 0.3 and ~ 1.0 , respectively) [*Stein and Stein*, 1994]. Seafloor heat-flow values below the conductive prediction are generally attributed to advective heat loss resulting from hydrothermal circulation within permeable basement. The sparse distribution of early data offshore Costa Rica precluded confident determination of the cause(s) of the observed heat-flow patterns.

Additional heat-flow measurements were collected near the MAT offshore of Costa Rica in the mid-1990s during a site survey in preparation for ocean drilling. *Langseth and Silver* [1996] collected >100 new heat-flow values organized mainly along several transects on the margin wedge and close to the trench axis on EPR-generated crust. Heat flow in the deepest part of the trench averaged 17 mW/m², and values on a fault-bounded bench seaward of the trench averaged 12 mW/m². Mean heat flow was somewhat higher, generally 25–30 mW/m², on the margin wedge within 30 km of the trench. This survey was conducted on and above oceanic crust produced entirely along the EPR, confirming with modern equipment that the low heat-flow values detected during previous decades were characteristic of this part of the Cocos plate.

Heat-flow data were collected at greater subseafloor depths during ODP Leg 170 [Kimura *et al.*, 1997]. The measured value within the trench at Site 1039 was 9 mW/m^2 , about half the value measured at this location using surface probes. Borehole values from higher up on the wedge were also considerably lower than those determined with shallow seafloor probes. The discrepancy between borehole and seafloor values can be reconciled if there is upward fluid seepage at rates of $5\text{--}20 \text{ mm/yr}$ [Ruppel and Kinoshita, 2000]. This rate of flow is too low to cause curvature in shallow thermal gradients measured close to the seafloor but will result in a significant reduction in conductive heat flow with depth [e.g., Bredehoeft and Papadopoulos, 1965; Fisher, 2004; Langseth *et al.*, 1988]. Langseth and Silver [1996] attributed the low heat flow on the incoming plate near Site 1039 to efficient hydrothermal cooling in basement, with the extent of cooling possibly being enhanced by reactivation of normal faults outboard of the MAT due to plate flexure. A similar hypothesis was applied to the incoming plate along the Peru Margin [Yamano and Uyeda, 1990]. Models of the thermal regime of the incoming plate on the Costa Rica margin that account for hydrothermal cooling are in general agreement with observations of a landward increase in surface heat flow across the margin wedge [Harris and Wang, 2002; Langseth and Silver, 1996; Spinelli and Saffer, 2004]. All three models are able to fit the observations reasonably well when hydrothermal circulation is assumed to penetrate $500\text{--}1000 \text{ m}$ into basement.

As of the late 1990s, thermal studies had established that EPR-generated seafloor northwest of the plate suture offshore of the Nicoya Peninsula was cooler than the global mean for crust of this age, whereas CNS-generated seafloor southeast of the plate suture was warmer than the global mean, but close to the conductive prediction. However, the available data did not permit determination of the location of the thermal transition between areas of warm and anomalously cool seafloor. As a result, the association of this transition with one or more tectonic boundaries and the cause(s) of the difference in seafloor thermal state remained uncertain. In addition, it was unclear how typical the ODP drilling transect was with respect to regional thermal conditions or how well two-dimensional thermal models of subduction might be expected to simulate subseafloor conditions. If there is a difference in the efficiency of hydrothermal heat extraction within EPR-generated seafloor, why does this occur? Why is the region of anomalously cool seafloor located within a segment that had been previously characterized as being "smooth," whereas the region of anomalously warm seafloor is located in an area that had been characterized as being "rough" [von Huene *et al.*, 2000]? This correlation is the opposite to what one might expect if the efficiency of hydrothermal heat extraction were enhanced by the presence of basement outcrops, since rougher seafloor might be expected to have more areas of basement exposure. Is it important that the overall structural "fabric" (as determined from magnetic lineations) of EPR-generated seafloor is oriented parallel to the trench, whereas CNS-

generated seafloor crustal structure trends perpendicular or oblique to the trench? Perhaps this difference in structural orientation influences the extent of fault reactivation during flexure outboard of the trench and thus leads to a difference in the development of enhanced permeability in basement. The TicoFlux program was designed to address these questions and to assess the nature of hydrothermal processes in this region.

The TicoFlux Program

The TicoFlux program included two expeditions to investigate the nature of hydrothermal activity and its influence on lithospheric and subduction processes on the Cocos plate. The first cruise (TicoFlux 1) focused on regional patterns and processes, and the second (TicoFlux 2) assessed the influence of seamounts, faults, and other local features in guiding hydrothermal fluid flow. Both programs focused on a $2^\circ \times 2^\circ$ region of the Cocos plate seaward of the MAT (fig. 4.1), where fundamental transitions in the structural, hydrological, and thermal state of the plate were thought to occur. Each expedition collected seismic, hydrosweep, and heat-flow data, as well as cores for analysis of sediment properties and pore-fluid geochemistry. The present paper focuses on preliminary thermal and limited seismic results; other TicoFlux work will be published elsewhere.

Data Acquisition and Processing We collected 1800 km of 480-channel seismic data during TicoFlux 1 and an additional 1200 km of four-channel data during TicoFlux 2. During TicoFlux 1, shots were generated with a 10-gun array and spaced 37.5 m apart. The 6000-m streamer provided 6.25-m hydrophone spacing and 80-fold subsurface coverage. During TicoFlux 2, shots were fired with two guns at 33.3-m intervals. The receiver cable consisted of four 50-m active sections and yielded threefold coverage. Data were processed initially aboard ship using SIOSEIS and later processing onshore was accomplished using SeisWorks. Hydrosweep data were edited manually to remove bad pings and noise. Data collected during TicoFlux 1 were combined with those collected by numerous other workers in the region (most of which was from landward of the trench) to generate a single bathymetric grid with 200-m pixel resolution (C. Ranero, personal communication, 2002). These data were overlain on coarser bathymetric data derived from satellite gravimetry, having a pixel resolution of ~ 3 km [Smith and Sandwell, 1997]. Hydrosweep data from TicoFlux 2 were draped across the composite data set.

Multipenetration heat-flow data were collected during both expeditions using a 3.5-m, 11-thermistor, violin-bow heat flow probe with in situ thermal conductivity [Hyndman *et al.*, 1979]. Heat-flow stations were colocated along seismic reflection profiles in order to merge information on sediment thickness and basement structure with thermal data. An additional 57 estimates of heat

flow were made using autonomous, outrigger temperature probes [Pfender and Villinger, 2002] attached to gravity and piston cores. Data were processed on the basis of techniques described by Villinger and Davis [1987]. We used a Monte Carlo analysis to assess uncertainties in heat-flow values resulting from ambiguity as to the thickness of sediment layers having differing thermal conductivities and used the “scatter” parameter to aid in assessing how many thermistors should be used for each heat-flow estimate [Stein and Fisher, 2001]. Outrigger data were analyzed using the same method, but we added an additional uncertainty in the Monte Carlo analysis to account for representation of thermal conductivity with a depth function rather than individual measurements associated with each core.

Extrapolation of Seafloor Heat-Flow Data to Depth We estimated thermal conditions within sediments and shallow basement across the field area using a method similar to that of Davis *et al.* [1999]. Heat-flow data were combined with seismic estimates of sediment thickness and thermal-conductivity data derived from drilling to extrapolate downward from the seafloor to uppermost basement. Sediment cores recovered from ODP Site 1039, on the incoming plate in the trench, were tested during Leg 170 to determine sediment thermal conductivity and seismic velocity at a core scale, and additional information on seismic interval velocities was available from synthetic seismograms and drilling data [Kimura *et al.*, 1997]. Uncertainties in estimated temperatures at depth are based on uncertainties in point measurements of heat flow, depth to basement as picked from seismic profiles, and thermal resistance versus travel time relations developed from drilling data.

A comparison between *P*-wave velocities measured on core samples and interval velocities determined from seismic and drilling data at ODP Site 1039. Kimura *et al.* [1997] demonstrated that the core measurements were essentially correct in the upper 180 m of hemipelagic sediment (mean velocity of 1570 m/s), but core measurements underpredicted seismic velocities by ~9% within the deeper, pelagic section (fig. 4.2a). We attribute this disparity to (1) damage to the core samples that commonly occurs during rotary drilling and is most pronounced in lithified materials that are readily cracked during recovery and handling and (2) systematic underrepresentation of coarse-grained (sandy) material in the recovered core.

We tested two options for correcting the seismic velocities: applying a constant offset of 9% and applying an offset whose magnitude increased linearly with depth within the pelagic section. Cumulative two-way travel time (*t*) was computed from individual shipboard measurements (*v*) weighted by the depth intervals (*dz*) between them

$$t(z) = \int_0^z \frac{dz}{v} \quad (4.1)$$

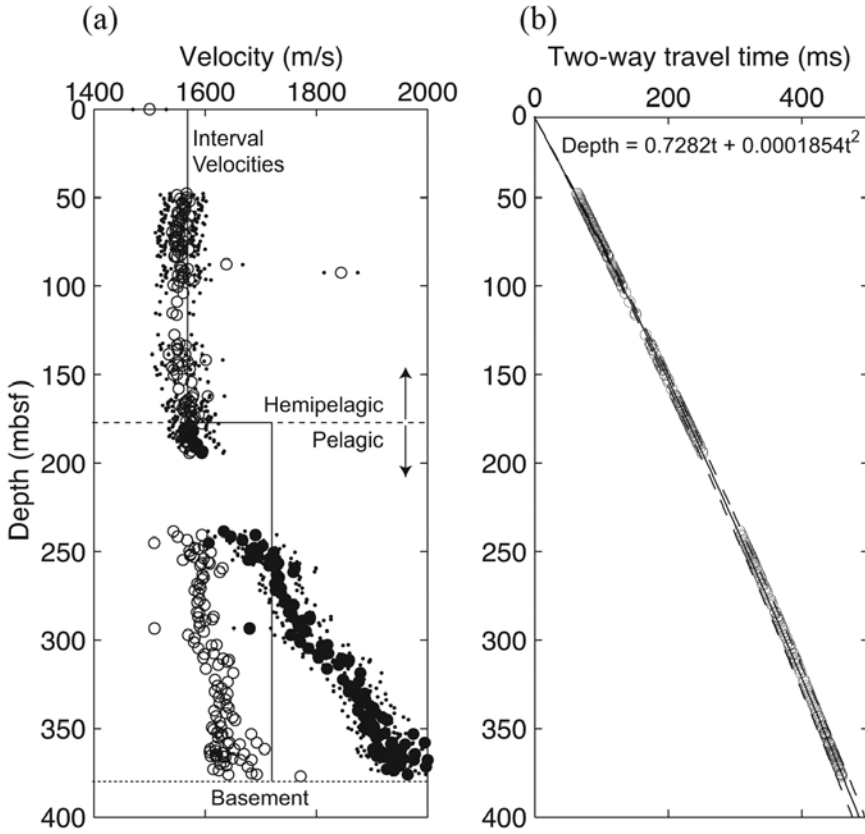


Figure 4.2 (a) Open circles show ODP shipboard seismic velocity measurements on cores recovered from ODP Leg 170 [Kimura *et al.*, 1997]. The pelagic/hemipelagic boundary occurs at a depth of 180 mbsf. Solid circles below the pelagic/hemipelagic boundary were adjusted linearly to be consistent with interval velocities obtained from synthetic seismograms. Single dots denote ± 1 standard deviation applied to data from above and below the pelagic/hemipelagic boundary. Solid lines indicate average seismic velocities for each section. (b) Cumulative travel time computed from individual shipboard measurements weighted by the depth interval between them. Solid line shows the fit of a second-order polynomial regression. Dashed lines show uncertainty by regressing the data with ± 1 standard deviation.

and regressed against depth below seafloor to derive the best-fitting, second-order polynomial function that allowed a transformation from two-way travel time to sediment thickness (fig. 4.2b). The function based on a depth-varying velocity correction resulted in a polynomial having a smaller second-order term, and we consider this to be preferable because it will help to minimize errors associated with extrapolation of the velocity-depth function beyond the sediment thickness at Site 1039 (~400 m). After applying the

correction described above, we further estimate an uncertainty in this time-to-depth conversion by shifting the seismic velocities by ± 1 standard deviation of the mean within each sediment interval.

The thermal conductivity of sediment cores recovered from Site 1039 was also determined on ODP Leg 170 [Kimura *et al.*, 1997] (fig. 4.3). Thermal-conductivity measurements are likely to be influenced by damage to the core much like seismic velocities, but we lack an independent estimate of upper-basement temperature that is necessary to apply rigorous corrections [e.g., Davis *et al.*, 1999]. Rather than attempting to correct thermal-conductivity values for core damage, we add an additional uncertainty to individual conductivity values [e.g., Bevington and Robinson, 1992] of ± 1 standard deviation of the mean

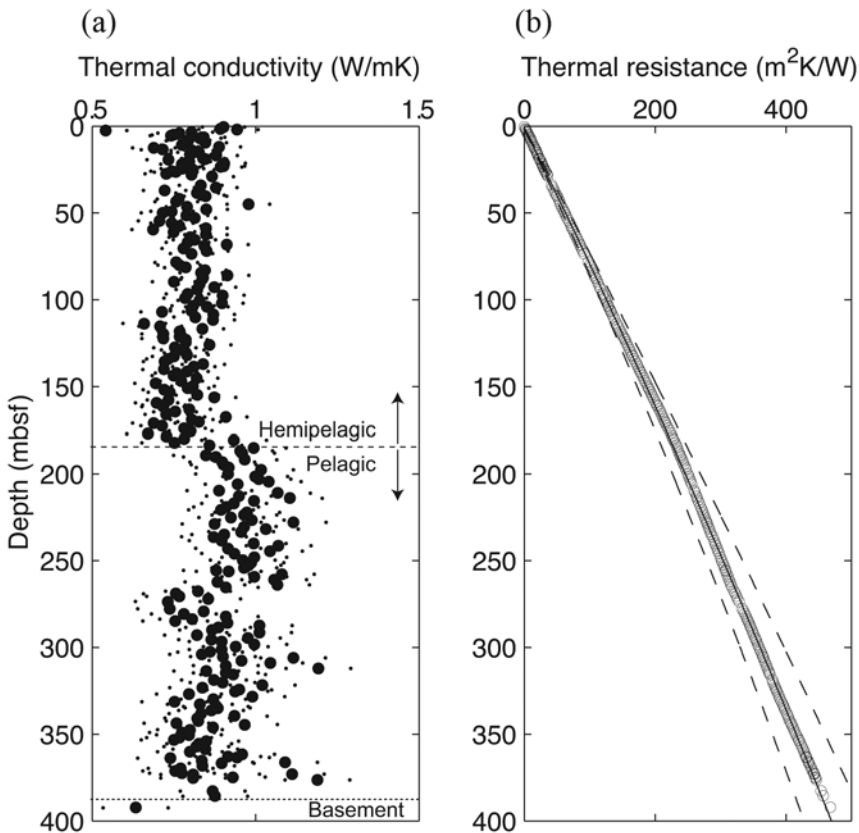


Figure 4.3 (a) Circles show ODP shipboard thermal conductivity measurements on cores recovered from ODP Leg 170 [Kimura *et al.*, 1997]. The pelagic/hemipelagic boundary occurs at a depth of 180 mbsf. Single dots denote ± 1 standard deviation applied to data from above and below the pelagic/hemipelagic boundary. (b) Cumulative thermal resistance computed from individual shipboard thermal conductivity measurements weighted by the depth interval between them. Solid line shows the fit of a second order polynomial regression. Dashed lines show uncertainty by regressing the data with ± 1 standard deviation.

thermal conductivity within each of the hemipelagic and pelagic intervals. Cumulative thermal resistance (R) was computed from individual shipboard measurements (λ) weighted by the depth intervals (dz) between them,

$$R(z) = \int_0^z \frac{dz}{\lambda} \tag{4.2}$$

and regressed against depth below seafloor to derive a function allowing for the transformation from sediment thickness to cumulative thermal resistance.

Uncertainties in seismic velocities and thermal conductivity described above generate combined uncertainties in thermal resistance versus two-way time (depth) of $\pm 10\%$. There are additional uncertainties in picking the upper-basement reflector from seismic data (varies from site to site, particularly where the upper-basement surface is steep), in individual heat-flow values, in extrapolation of Site 1039 seismic velocity and thermal-conductivity data across the field area, and in the assumption that heat transport within the sediment is one-dimensional and vertical. Collectively, these factors may lead to uncertainties in the temperature at the sediment-basement interface and in the locations of isotherms within the sediment section, of 15–25% (fig. 4.4).

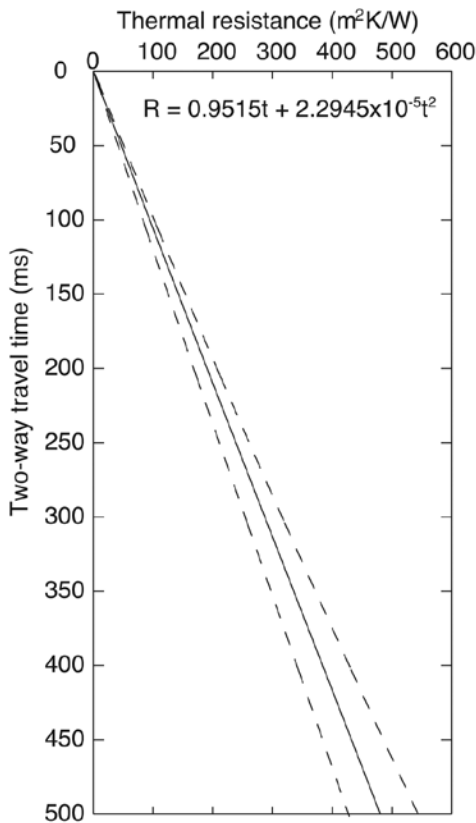


Figure 4.4 Relationships between cumulative thermal resistance and sediment two-way travel time resulting from regressions in figures 4.2 and 4.3. Solid line shows the fit of a second-order polynomial regression, and dashed lines show uncertainty from regressions where ± 1 standard deviation had been applied. As sediment two-way travel time increases, the fractional difference in the uncertainty in cumulative thermal resistance remains constant at roughly 8.5%. We apply a conservative 10% uncertainty in cumulative thermal resistance to all calculations of temperatures along the sediment-basement interface.

Thus it is risky to draw conclusions from individual temperature estimates. Instead, we focus on trends apparent in profiles of extrapolated temperatures and temperature contours, all of which are subject to the same assumptions and limitations.

In the absence of additional physical property data, the thermal structure within oceanic basement is even less well-constrained. For illustrative purposes, and in order to continue extrapolated temperature contours below the sediment-basement interface, we assume a thermal conductivity of upper-basement rocks of 1.6 W/m-K [e.g., *Becker et al.*, 1983; *Busch et al.*, 1992; *Karato*, 1983] and *P*-wave velocity of 4500 m/s [e.g., *Carlson*, 1998; *Jacobson*, 1992; *Rohr*, 1994]. However, vigorous local circulation may homogenize temperatures locally within upper basement [e.g., *Davis et al.*, 1989; *Fisher et al.*, 1990; *Langseth and Herman*, 1981], so temperature contours within upper basement should be viewed cautiously.

Thermal and Related Analyses

The focus of this section is on variations in thermal conditions within sediments and uppermost basement across the TicoFlux survey area. We begin with a brief assessment of seafloor and basement relief, as this topic is important for understanding the distribution of warmer and cooler crustal areas. Next, we show examples of heat flow and seismic transects across tectonic boundaries, thermal transitions, faults, and buried and exposed basement highs. Individual profiles are shown with thermal data and interpretations superimposed on seismic data, with line locations shown in figure 4.1. These examples are not exhaustive but illustrate characteristic patterns that help in delineating the thermal structure of the upper oceanic crust in this area. Finally, we conclude by discussing what these features and thermal patterns mean for local and regional hydrothermal conditions in basement, how the thermal state of the subducting crust could impact the seismogenic zone below the Nicoya Peninsula.

Seafloor and Basement Relief

On the basis of newly acquired hydrosweep coverage, seamounts are common features on EPR-generated seafloor (fig. 4.1) north of the plate suture. The largest of these features were apparent in bathymetric data derived from satellite gravimetry prior to the TicoFlux program [e.g., *Wessel*, 2001], consisting of massive edifices 3–5 km or more in diameter and rising 1–2 km above the surrounding seafloor. Swath data collected during the TicoFlux expeditions confirmed (or shifted) the locations of these features and identified numerous smaller basaltic outcrops that were not apparent from the satellite data. Because the spacing between seamounts in this area is typically several to tens

of kilometers, a randomly positioned seismic line is unlikely to cross a basaltic outcrop. It is therefore not surprising that outcrops are relatively uncommon features on seismic data collected prior to swath mapping. High-resolution TicoFlux seismic data further revealed numerous buried basement highs that were outcrops before being covered by accumulating sediment. These local basement highs (buried or exposed at the seafloor) were found to be relatively common on EPR-generated seafloor in this area, whereas CNS-generated seafloor immediately adjacent to the plate suture and MAT appears to be entirely devoid of both exposed seamounts and large buried basement highs (fig. 4.1). Continuing to the south, across the ridge jump and propagator trace, seamounts and outcrops become much more prominent in association with the Cocos Ridge.

Heat-Flow Transects and Seismic Profiles

Thermal Transitions and Tectonic Boundaries Heat-flow station TF1-HF02 comprises 12 heat-flow measurements collocated along seismic line TF1-07, crossing the ridge jump near 87°03'N, 8°22'W (figs. 4.1 and 4.5). Basement is generally flat below 400 m of sediment, except for a 1000-m-wide, 160-m-tall buried basement high that corresponds to the ridge-jump trace.

Measured heat flow is 112–124 mW/m² across the transect, consistent with predictions from lithospheric cooling models for 19–21 Ma seafloor. Extrapolated temperatures along the sediment-basement interface remain generally uniform at 51°–59°C, except at the ridge jump where the estimated upper-basement temperature is just 35°C. This temperature estimate is consistent with purely conductive conditions; the lower value results from shallowing of basement coupled with slight thermal refraction, and there is no thermal evidence for hydrothermal processes in basement on either side of the ridge jump.

Conditions are markedly different along heat-flow station TF1-HF06. This station consisted of 13 heat-flow measurements collocated along seismic line TF1-14, crossing the propagator trace near 86°4'W, 8°23'N (figs. 4.1 and 4.6). As along line TF1-07 traversing the ridge jump to the west, basement is generally flat with the exception of a 2000-m-wide, 200-m-tall buried basement high associated with the propagator trace. Heat flow varies between 104 and 128 mW/m² along most of the transect but is elevated to >200 mW/m² above the propagator trace. Extrapolation of seafloor thermal conditions to depth indicates a relatively consistent temperature at the sediment-basement interface across this transect of 32°–41°C (essentially constant within estimated uncertainties), with only slightly lower apparent temperatures above the propagator trace. The consistency of temperatures across and adjacent to the propagator trace, despite a 200-m difference in elevation of the top of basement, requires that heat be redistributed efficiently within basement in this area, most likely by hydrothermal circulation. Similar processes have been documented in other

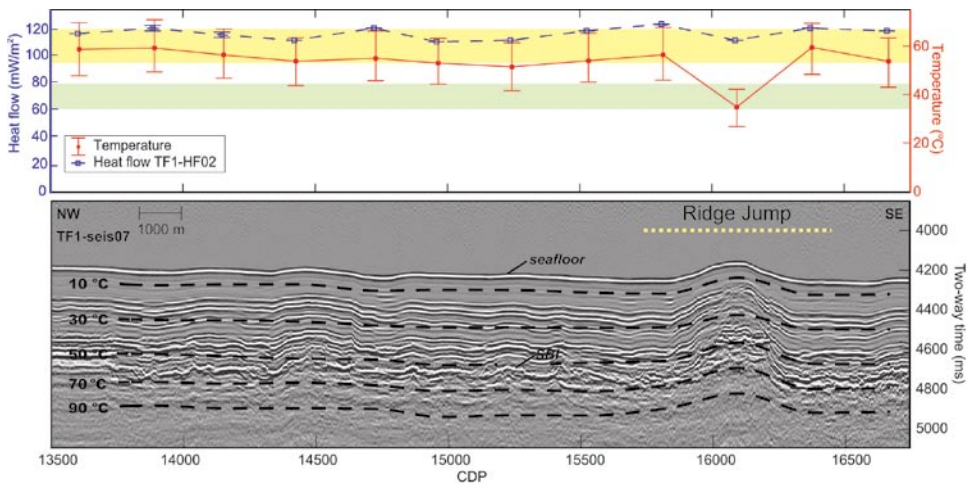


Figure 4.5 Seismic, heat flow, and calculated temperature data traversing the ridge jump along TF1-seis07. Top panel shows measured seafloor heat flow (blue squares) and calculated sediment-basement interface temperatures (red circles), with yellow and green bands indicating the conductive prediction and global mean, respectively, for heat flow through 18–24 Ma seafloor. Bottom panel shows seismic data overlain by isotherms calculated from heat flow and cumulative thermal resistance relationships shown in figure 4.4. The tectonic transition from *Barckhausen et al.* [2001] is centered along the buried basement high at CDP 16100. The seafloor and sediment-basement interface (SBI) are highlighted. Heat flow remains relatively constant across the transition while the sediment basement temperature decreases, indicative of vertical heat conduction and no hydrothermal fluid flow.

ridge-flank sites where vigorous circulation in upper basement homogenizes basement temperatures [e.g., *Davis et al.*, 1992; *Fisher et al.*, 1990]. There is no evidence for advective heat loss from the crust along heat-flow station TF2-HF06; all heat associated with lithospheric cooling is accounted for in the measured seafloor values. Instead, vigorous convection in basement moves heat around locally, elevating temperatures in upper basement along the propagator trace and increasing seafloor heat flow above this feature. This condition contrasts strikingly with that seen along heat-flow transect TF1-HF02 across the ridge jump (fig. 4.5), where thermal conditions are completely conductive.

In both of these examples, there are no thermal transitions associated with the major tectonic boundaries; both boundaries occur within “warm” parts of the plate, where heat flow is approximately that predicted by conductive lithospheric cooling models. Heat-flow transect TF1-HF02 crosses between seafloor created at the EPR and seafloor generated at the CNS, and conditions on both sides of the ridge jump are entirely conductive (fig. 4.5). Heat-flow transect TF2-HF06 crosses a propagator trace entirely within CNS-generated

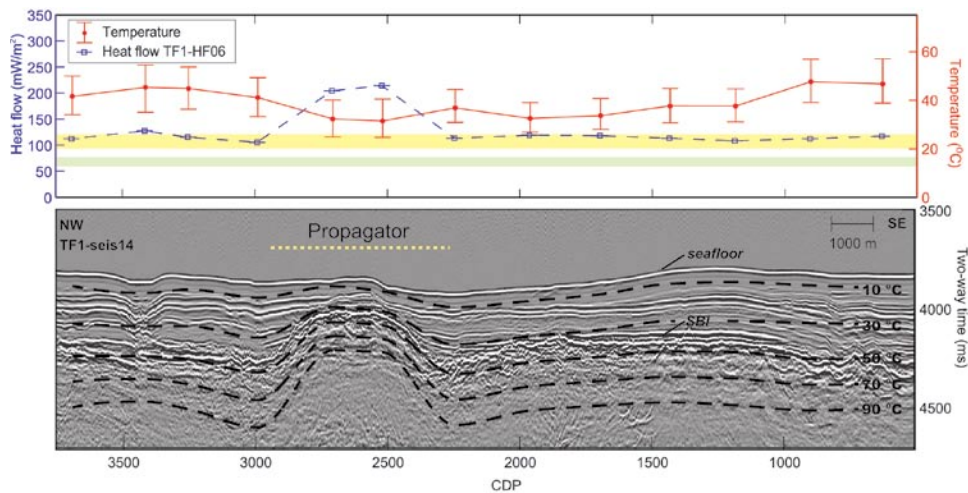


Figure 4.6 Seismic, heat flow, and calculated temperature data traversing the propagator trace along TF1-seis14. Symbols and nomenclature are the same as figure 4.5. Heat flow more than doubles across the buried basement high centered at CDP 2600, while sediment thins to roughly 100 m. Temperatures along the sediment-basement interface remain relatively uniform around 37°C across the basement high, indicating vigorous hydrothermal circulation within the feature.

seafloor, and hydrothermal circulation redistributes heat locally within this feature (fig. 4.6).

We found one thermal transition during the TicoFlux expeditions that corresponds to a tectonic boundary between different parts of the Cocos plate. Heat-flow station TF1-HF08 consisted of 11 heat-flow measurements collocated along seismic line TF1-11, crossing the triple-junction trace near 86°21'W, 9°0'N (figs. 4.1 and 4.7).

The top of basement is ~100 m shallower on CNS-generated seafloor than on EPR-generated seafloor, with the change in depth occurring across a lateral distance of 1.5 km. Seafloor heat flow is ~30 mW/m² on the northwest (EPR) side of the transect and rises to ~100 mW/m² on the southeast (CNS) side. Temperatures along the sediment-basement interface on the EPR side of the boundary are 15°–30°C (rising with proximity to the boundary), whereas upper-basement temperatures on CNS side approach 45°C, even though the basement is shallower. Similar thermal transitions have been modeled by Fisher *et al.* [2003b], and as discussed below, the abruptness of this thermal transition (heat flow varies by a factor of 3 over a lateral distance of <3 km) suggests that it results from shallow hydrothermal circulation within the uppermost crust.

Other Thermal Transitions Most thermal transitions documented during the TicoFlux program were not associated with any tectonic boundary [Fisher *et al.*,

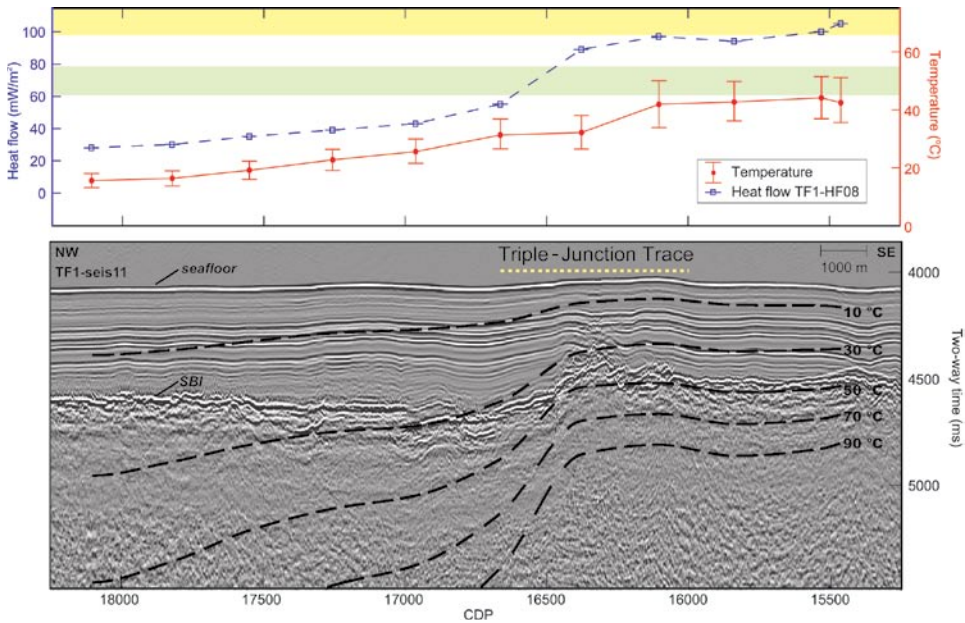


Figure 4.7 Seismic, heat flow, and calculated temperature data traversing the triple junction trace from EPR- to CNS-generated crust along TF1-seis11. Symbols and nomenclature are the same as fig. 4.5. Heat flow increases from suppressed values around 30 mW/m² on the EPR side to over 100 mW/m² on the CNS side. Isotherms are severely depressed on EPR-generated crust, indicative of efficient removal of large portions of lithospheric heat.

2003b] (fig. 4.1). As an example, heat-flow stations TF1-HF03,10,09 comprising 27 heat-flow measurements collocated along seismic line TF1-13, are entirely on EPR-generated seafloor and ~40 km from the nearest tectonic boundary (fig. 4.8).

Seafloor topography across the transect is generally flat, with bathymetric relief <50 m and sediment thicknesses of 350–450 m. The reflection character of basement in the northwestern part of the transect consists of a high-amplitude, generally smooth surface, which may be indicative of widely distributed sills near the base of the sediments [Fisher *et al.*, 2003b]. This area of smooth basement ends abruptly near CDP 9650, abutting a 4000-m-wide, 150 m-tall basement high. On the southeast side of this feature, the upper-basement reflector is much less distinct, and basement relief is considerably rougher.

The transition in basement appearance coincides with a rapid transition in seafloor heat flow, with values increasing from <30 mW/m² to the northwest to >100 mW/m² over a lateral distance of <2 km. Corresponding temperatures along the sediment-basement interface increase from <20°C to >40°C, from northwest to southeast. The abruptness and magnitude of this thermal transition indicates an extreme contrast in the nature and extent of heat loss from the upper oceanic crust in this area, with 70% of lithospheric heat being extracted

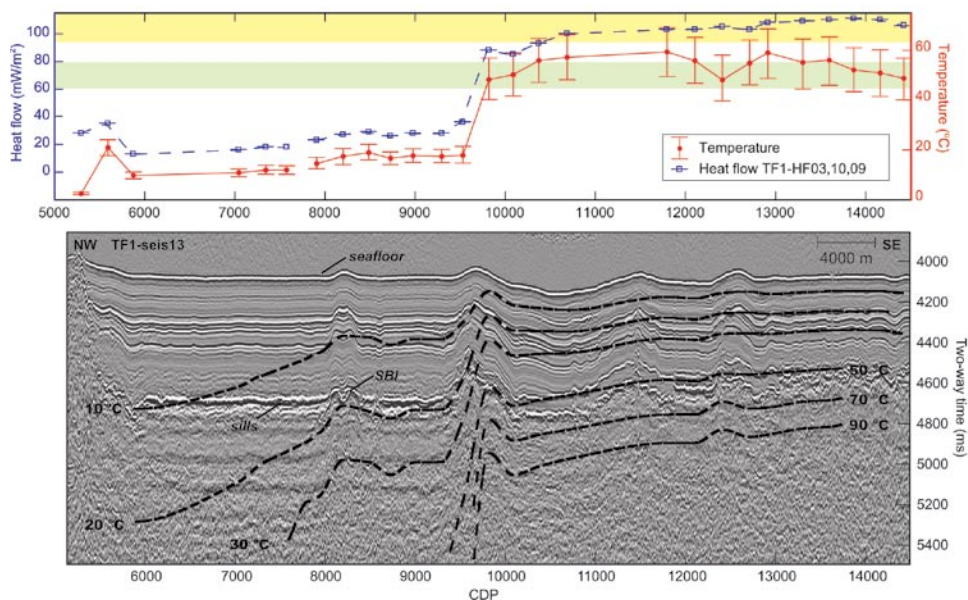


Figure 4.8 Seismic, heat flow, and calculated temperature data along TF1-seis13 on EPR-generated crust. Symbols and nomenclature are the same as figure 4.5. Heat flow transitions abruptly from <30 to >100 mW/m^2 over a lateral distance <2 km, while temperatures along the sediment-basement interface change concurrently. The abruptness and degree of this thermal transition indicate an extreme contrast in the nature and extent of hydrothermal circulation in shallow basement. The high-amplitude, smooth surface along the SBI is likely indicative of widely distributed sills.

from crust on the northwest side of this transect, most likely by hydrothermal circulation. In a later section, we discuss how local outcrops may facilitate rapid fluid exchange between the crust and ocean, cooling vast areas of EPR-generated seafloor in this region.

Heat-flow stations TF2-HF17 and TF1-HF05 comprise 22 heat-flow measurements collocated along seismic line TF1-03, with the two stations separated by an along-track distance of ~ 34 km (figs 4.1 and 4.9).

Basement is generally flat along transect TF2-HF17 and is covered with ~ 400 m of sediments (fig. 4.9a). Measured heat flow is $102\text{--}107$ mW/m^2 , consistent with predictions from conductive lithospheric cooling models for crust of this age. Extrapolated temperatures along the sediment-basement interface remain generally uniform at $48^\circ\text{--}55^\circ\text{C}$. These thermal data are entirely consistent with purely conductive conditions.

Heat-flow and sediment-basement interface temperatures drop by $\sim 80\%$ 34 km northeast at station TF1-HF05 (fig. 4.9b), which crosses four fault-bounded benches immediately southwest of the ODP Leg 170 drilling transect (fig. 4.1). Station TF1-HF05 consisted of 12 heat-flow measurements extending roughly 15 km into the trench. Overall seafloor depth increases from ~ 3600 to over

4200 m, while seafloor relief across the faults ranges between 25 and 130 m. Basement relief varies between 50 and 140 m, with the largest offsets corresponding to faults closer to the trench axis. Sediment thickness across the transect is very uniform at 380–400 m. Heat-flow values range between 13 and 35 mW/m², with values elevated locally directly above basement faults. Extrapolated temperatures along the sediment-basement interface decrease from >12°C to <8°C from southwest to northeast along this transect.

Although the exact location and extent of the thermal transition along seismic line TF1-03 was not identified, the 80% decrease in lithospheric heat flow between stations TF2-HF17 and TF1-HF05 indicates an extreme contrast in the character and extent of heat extraction along a profile perpendicular to the MAT. Bend-related normal faults have been suggested to create permeable pathways allowing fluids to hydrate the lower crust and upper mantle in similar settings [Peacock, 2001; Ranero *et al.*, 2003]. The pervasiveness of bend-related faults along the trench slope outboard of the MAT on EPR-generated crust is hypothesized to provide pathways for deep penetration of seawater and an efficient mechanism for considerable lithospheric heat extraction. The influx of seawater is thought to promote serpentinization of chemically reactive lithospheric mantle and crust, leading to physical and chemical changes within the subducting slab. An important by-product of serpentinization is the generation of substantial amounts of heat [e.g., Kelley *et al.*, 2001; Lowell and Rona, 2002], and we would expect to see some evidence of this (either as direct fluid venting or as increased conductive heat flow) at the seafloor. If additional heat were being generated by serpentinization within the upper lithosphere and mantle in this region, then this additional heat must also be efficiently mined by hydrothermal circulation.

In order to investigate the origin of locally elevated heat-flow values measured above faults along heat-flow transect TF1-HF05 (fig. 4.9b), we constructed a two-dimensional finite element model using Finite Element Heat and Mass (FEHM) [Zyvoloski *et al.*, 1996]. Our model domain consisted of a 20-km grid, with eight sedimentary and six basalt units (seafloor and sediment-basement interface horizons were digitized from seismic line TF1-03), and a typical horizontal node spacing of 25 m. Physical properties from ODP Leg 170 Hole 1039 [Kimura *et al.*, 1997] were used as model constraints. Model output from a purely conductive simulation shows locally elevated heat flow of roughly 10–40% above the faults, with the largest increases corresponding to the greatest seafloor relief changes near CDP's 2050 and 2625, in the central portion of the transect (fig. 4.9b). We conclude that seafloor thermal refraction alone is sufficient to explain the locally elevated heat flow measured above the faults, and there is no evidence for either thermally significant subvertical fluid flow or serpentinization at depth.

Variations in Heat Flow Around Buried Basement Highs It is well known that basement relief enhances hydrothermal circulation and heat advection within

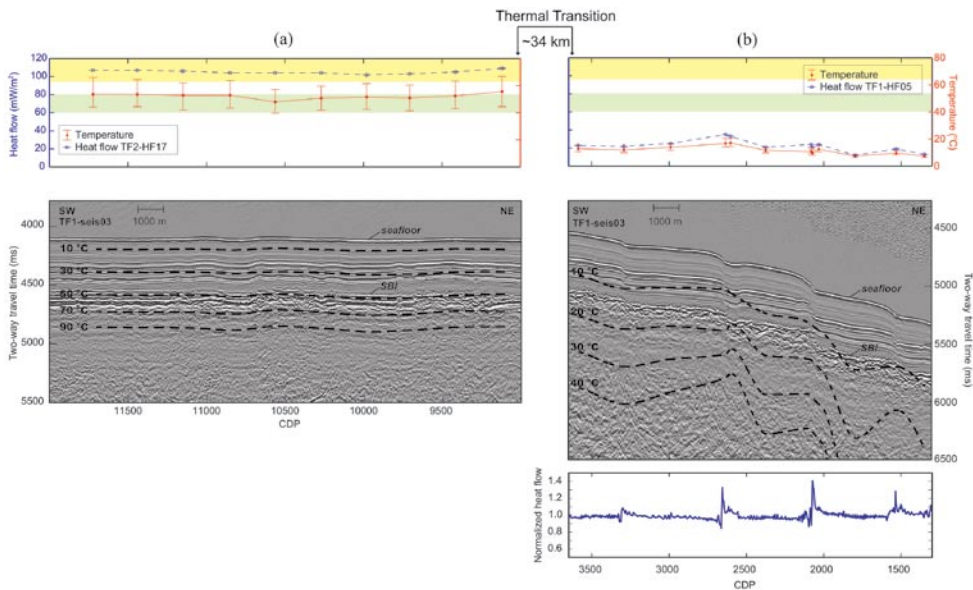


Figure 4.9 Seismic, heat flow, and calculated temperature data along TF1-seis03 (orientated perpendicular to the MAT) on EPR-generated crust. Symbols and nomenclature are the same as figure 4.5. (a) Station TF2-HF17 heat flow remains uniform across the transect at ~ 110 mW/m², and temperatures along the SBI remain constant at $\sim 55^\circ\text{C}$. A significant thermal transition occurs along the 34 km separating stations TF2-HF17 and TF1-HF05, where heat flow drops by $\sim 80\%$. (b) Station TF2-HF05 crosses four fault-bounded benches extending ~ 15 km seaward of the MAT. Heat flow varies between 12 and 35 mW/m², with locally elevated values corresponding to locations directly above the faults. Temperature along the SBI varies between 8° and 18°C . Bottom panel shows results from a two-dimensional conductive model simulation, indicating that the locally elevated heat flow values above the faults are the result of seafloor thermal refraction, and not due to vertical fluid flow.

upper oceanic crust [e.g., *Davis et al.*, 1989; *Fisher et al.*, 1990; *Johnson et al.*, 1993; *Lowell*, 1980] by focusing fluid flow toward basement highs. In the TicoFlux area we find areas on both EPR- and CNS-generated seafloor where vigorous hydrothermal circulation associated with buried basement highs homogenizes basement temperatures. We have already shown one example of this phenomenon on CNS-generated seafloor (fig. 4.6), where the mean heat flow is roughly equal to the conductive prediction, and in this section we show two additional examples from EPR-generated seafloor that demonstrate the variability and extent of this process.

The most dramatic example of thermal homogenization occurs on heat-flow stations TF1-HF04,11, which consisted of 17 heat-flow measurements co-located along seismic line TF1-05 (figs. 4.1 and 4.10).

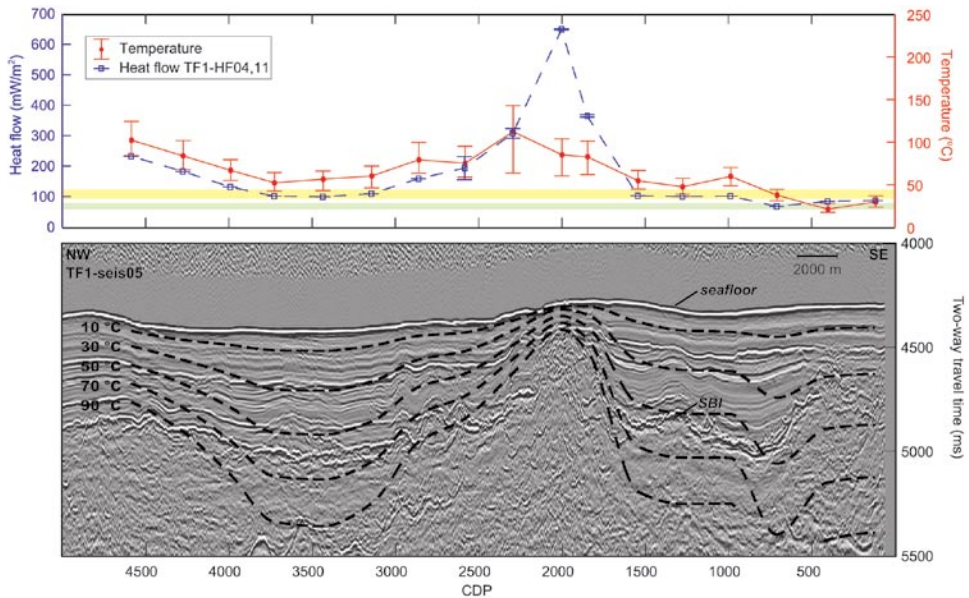


Figure 4.10 Seismic, heat flow, and calculated temperature data along TF1-seis05 on EPR-generated crust over an anomalously warm region. Symbols and nomenclature are the same as figure 4.5. Heat flow away from the basement high roughly matches conductive lithospheric cooling predictions for crust of this age, while over the basement high it rises by over sixfold as sediment thins to <100 m. Temperatures along the SBI remain remarkably uniform over the basement high despite the >500 m basement elevation change, indicative of vigorous hydrothermal circulation resulting in thermal homogenization within uppermost basement.

Seafloor heat flow is generally 30 mW/m² on EPR-generated seafloor in this region, but stations TF1-HF04,11 are in an isolated area where heat flow is considerably greater. Seafloor relief is <75 m along this transect, whereas a buried basement high rises by >550 m and sediment thins to <80 m above a 2.5-km-wide buried basement high. Heat flow rises along with basement elevation, from <100 to >650 mW/m², while estimated upper-basement temperatures remain remarkably uniform at ~80°C. The consistency of these temperatures requires vigorous fluid circulation. In the absence of hydrothermal circulation to homogenize upper-basement temperatures, we would expect to see a temperature difference of 50°–60°C between the shallowest and deepest basement along this heat-flow transect. The occurrence of such vigorous hydrothermal circulation requires considerable permeability in basement, in addition to heating from below, but it is not clear why this small area is also unusually warm relative to the surrounding seafloor. As discussed later, there is a large-scale flow system that extracts the majority of crustal heat from EPR-generated seafloor in this area on a regional basis, but it appears that the

crust in the vicinity of this buried basement high is not hydrologically well-connected to the larger-scale flow system.

Another example of thermal homogenization around a buried basement high on EPR-generated seafloor occurs on heat-flow transect TF2-HF01, which consisted of 17 heat-flow measurements colocated along seismic line TF1-11 (figs. 4.1 and 4.11).

Seafloor relief is less than 25 m along this transect, whereas the top of basement rises 300 m and sediment thins to ~275 m above a 1000-m-wide basement high. Heat flow along most of the transect is suppressed by roughly 70% relative to conductive lithospheric cooling models, but heat flow is locally elevated immediately above the buried basement high, rising to >60 mW/m². Temperatures along the sediment-basement interface over the entire transect remain extremely uniform around 25°C, including the basement high, indicating vigorous circulation in uppermost basement. This profile is very similar to profile TF2-HF06 on CNS-generated seafloor (fig. 4.6) except that the “background” heat-flow value, away from the buried basement high, is lower. Along both profiles, heat flow doubles immediately above the basement high as a result of local circulation.

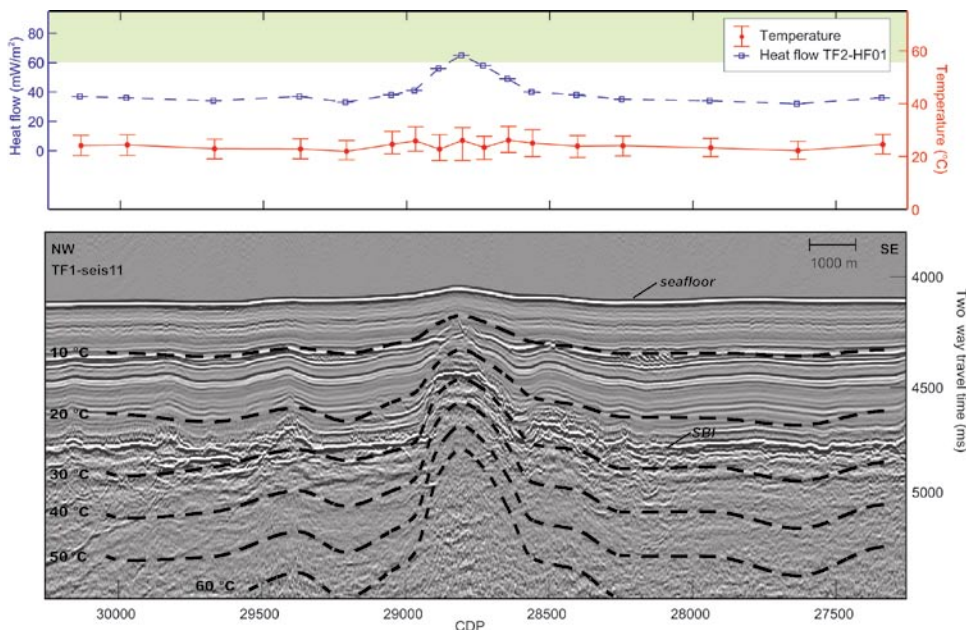


Figure 4.11 Seismic, heat flow, and calculated temperature data along TF1-seis11 on EPR-generated crust. Symbols and nomenclature are the same as figure 4.5. Heat flow doubles above the basement high centered at CDP 28800, while sediment thins to ~300 m. Hydrothermal circulation in uppermost basement is evidenced by temperatures along the SBI remaining extremely constant above the basement high, as is the case with TF01-HF(04,11) on seismic line TF1-05 (fig. 4.10).

Heat-Flow Measurements Near Discharging and Recharging Outcrops Seamounts and other basaltic basement outcrops are common on EPR-generated crust within the TicoFlux study area and are notably absent on CNS-generated seafloor southwest of the plate suture. These features appear to provide permeable pathways for the advective exchange of fluids and heat between the crust and overlying ocean, allowing hydrothermal fluids to bypass low-permeability sediments and efficiently extract large amounts of lithospheric heat [e.g., Fisher *et al.*, 2003a; Villinger *et al.*, 2002]. Modest pressure differences at the base of recharging and discharging columns of water provide the driving force for fluid exchange in this ridge-flank setting, and it is not possible to move fluids on a crustal scale at thermally significant rates through sediments thicker than a few meters [e.g., Davis and Becker, 2002; Fisher and Becker, 2000; Giambalvo *et al.*, 2000; Mottl and Wheat, 1994]. In this section, we present examples of heat-flow patterns around a discharging and a recharging seamount.

Fuente seamount is located on EPR-generated crust 56 km northwest of the intersection between the fracture zone and triple junction trace (figs. 4.1 and 4.12).

This conical feature has a radius of 2.5 km and rises 600 m above the surrounding seafloor. It was not apparent on bathymetric maps derived from

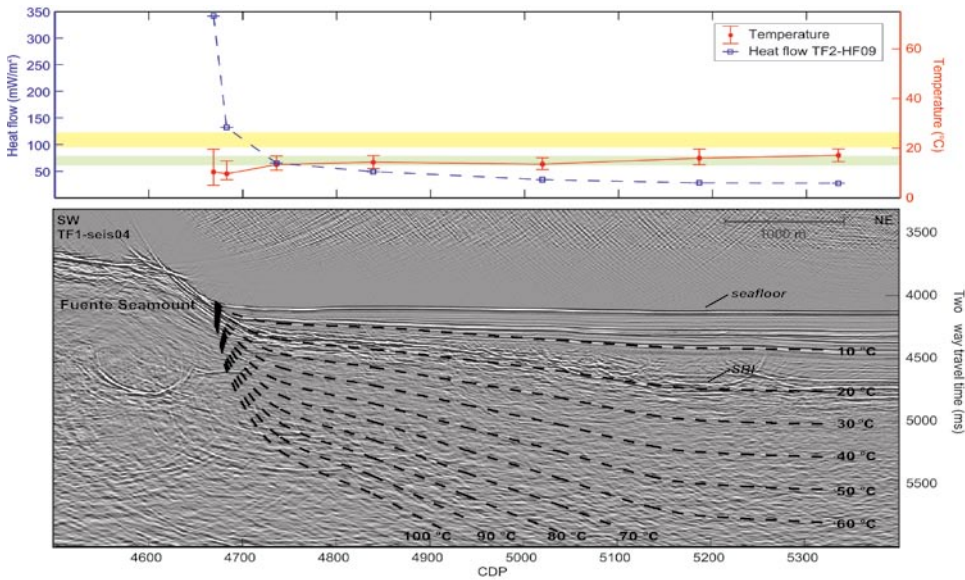


Figure 4.12 Seismic, heat flow, and calculated temperature data along TF1-seis04 crossing Fuente seamount. Symbols and nomenclature are the same as figure 4.5. Heat flow away from the outcrop is $<30 \text{ mW/m}^2$, and increases by over 10-fold at the edge of basement exposure. Projected isotherms dip subparallel to the SBI where temperatures remain relatively constant, indicative of lateral advection of hydrothermal fluid in uppermost basement. A recharging outcrop is shown in figure 4.13.

satellite gravimetry data but was discovered during seismic and swath-map surveys during TicoFlux 1. Seafloor topography is extremely flat in the region surrounding Fuente seamount, whereas basement shoals by over 500 m before reaching the seafloor. Heat-flow station TF2-HF09 consisted of seven measurements colocated along seismic line TF1-04 and was intended to map the heat-flow distribution within several kilometers of the seamount (fig. 4.12). Heat flow ≥ 2.5 km from the limit of basement exposure is <30 mW/m², consistent with regional values on EPR-generated seafloor, but rises rapidly to 340 mW/m² (>10 -fold) near the edge of the edifice. This increase in heat flow is several orders of magnitude greater than that which can be accounted for by conductive refraction alone. Temperatures along the sediment-basement interface remain remarkably constant at $\sim 15^\circ\text{C}$ along the entire length of the transect. If conditions in basement were conductive, we would expect to see a decrease in basement temperature as basement shallows upon approaching the outcrop. The data suggest instead that hydrothermal circulation locally homogenizes basement temperatures and are likely indicative of rapid lateral fluid flow toward (and out of) the seamount. Basement fluid temperatures are likely to be too low to generate a significant thermal anomaly in the water column around Fuente seamount, and venting fluids probably have a chemistry very close to bottom seawater because of the low temperature of reactions in basement [e.g., *Elderfield et al.*, 1999; *Kimura et al.*, 1997; *Mottl and Wheat*, 1994; *Wheat and Mottl*, 1994].

Tengosed seamount is located on EPR-generated crust 46 km northwest of the fracture zone trace and 44 km northeast of Fuente seamount (figs. 4.1 and 4.13).

This conical feature has a radius of 4.25 km and rises 1150 m above the surrounding seafloor. Unlike Fuente seamount, Tengosed is large enough to be readily apparent on bathymetric maps generated from satellite gravity data. Heat-flow station TF2-HF05 consisted of 21 stations colocated along seismic line TF2-23b, extending radially 12 km from the southern side of the seamount. In contrast to conditions around discharging Fuente seamount, heat flow near Tengosed decreases from >80 to <8 mW/m² over a lateral distance of roughly 7 km. In the absence of any significant variations in sediment thickness, temperatures along the sediment-basement interface are very low immediately adjacent to the outcrop, only slightly warmer than bottom water, and rise with increasing radial distance from the edifice. This pattern of suppressed heat flow and basement temperatures near the edge of the outcrop is indicative of substantial entrainment of cold seawater into upper basement, severely suppressing isotherms out to >4 km from the limit of basement exposure. This heat-flow profile is further complicated by the presence of a non-tectonic thermal transition occurring roughly 6 km from the outcrop around CDP 860, where most of the change in heat flow occurs over a lateral distance of 2–3 km.

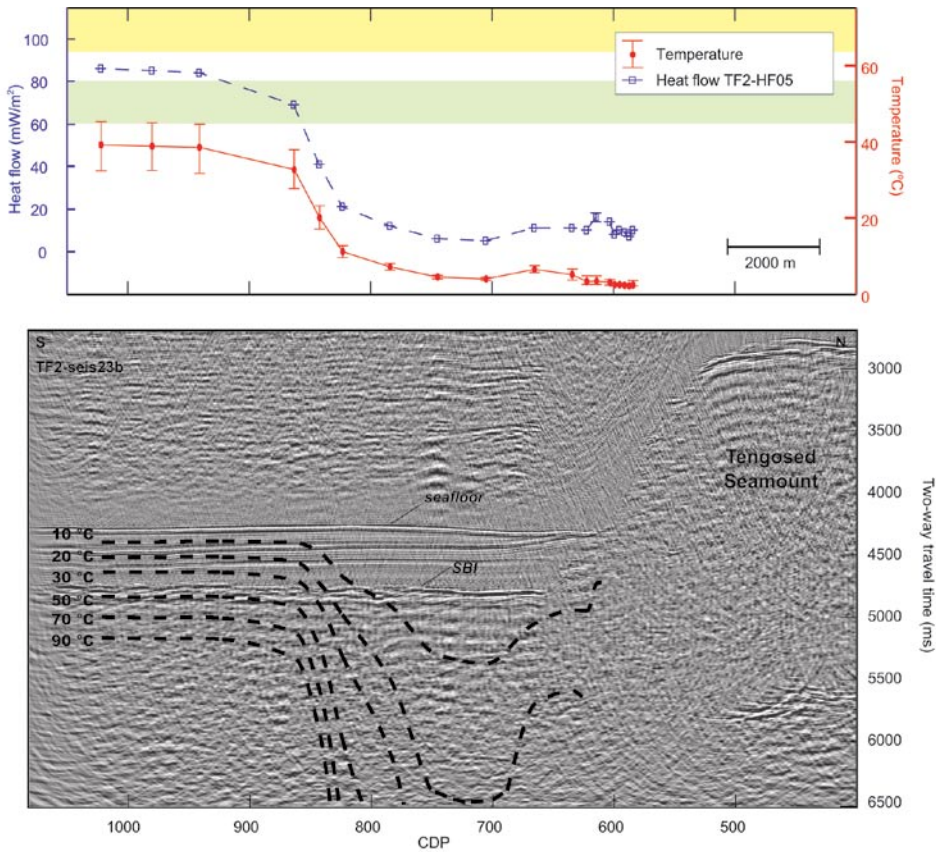


Figure 4.13 Seismic, heat flow, and calculated temperature data along TF2-seis23b crossing Tengosed seamount. Symbols and nomenclature are the same as figure 4.5. Heat flow in the vicinity of the outcrop drops by over 10-fold with temperatures along the SBI dropping concurrently. Isotherms in the vicinity of the outcrop are depressed out to 8 km from the limit of basement exposure, consistent with cold seawater being entrained and recharged into uppermost basement.

Hydrothermal Processes and Thermal Transitions

In order to evaluate the depth to the “source” of cooling within EPR-generated seafloor in the TicoFlux area, Fisher *et al.* [2003b] used numerical models of two-dimensional cross sections of the upper lithosphere within the Cocos plate. Heat was input into the base of the model domain, and heat sinks were distributed at various depths to simulate the extraction of heat by rapidly flowing hydrothermal fluids (fig. 4.14a).

Heat sinks were used to represent the advective extraction of heat without requiring specification of flow paths, three-dimensional modeling, or other

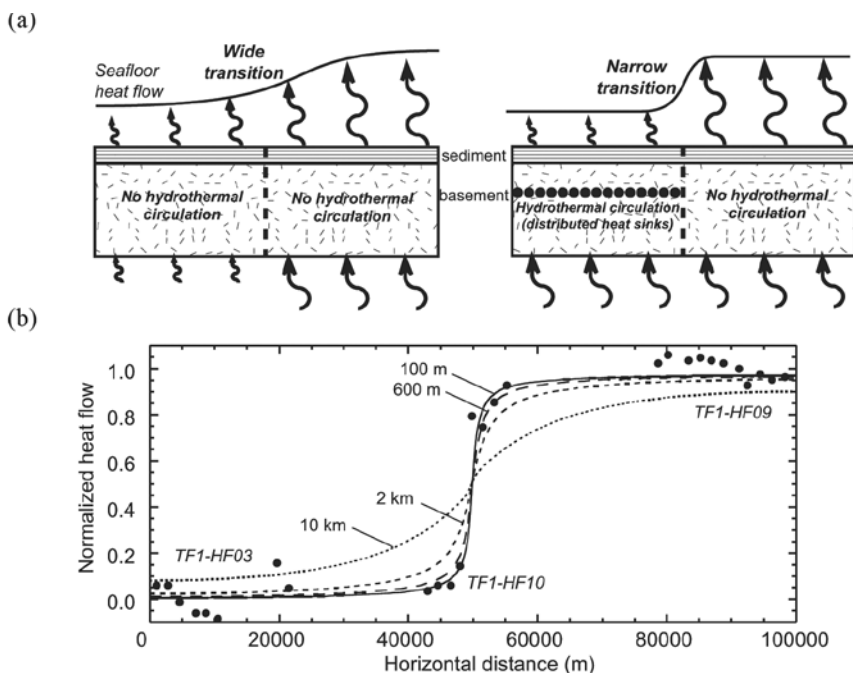


Figure 4.14 Conceptualization and results of models used to determine whether hydrothermal circulation was required within EPR-generated seafloor and to estimate the depth to the top of the hydrothermally active region [Fisher *et al.*, 2003b]. (a) Cartoons illustrating how the occurrence and depth to the top of the hydrothermal layer were tested. If the difference in seafloor heat flow detected on CNS- and EPR-generated seafloor resulted from differences in input at the base of the plate (or other deeply seated processes), we would expect to see a broad, gradual transition between warm and cool sides of the thermal transition. Alternately, if shallow hydrothermal circulation were responsible for the thermal contrast (as represented by point sinks for heat distributed on the left side of the transition), the transition should be narrow and abrupt. (b) Results of modeling of heat flow transect TF1-HF03,10,09 (fig. 4.8). Heat-flow values were normalized on a scale of 0–1, representing heat flow of 30–104 mW/m², for comparison to models. The abruptness and narrowness of the thermal transition requires relatively shallow hydrothermal circulation, a result consistent with modeling of other transitions in this area.

complexities. Fisher *et al.* [2003b] showed two seismic profiles and heat-flow transects across thermal transitions and compared observations to model predictions. We add results from another comparison between models and observations, based on heat-flow stations TF1-HF03,10,09 (figs. 4.8 and 4.14b). As with the other thermal transitions, the rapid increase in heat flow from ~30 to ~100 mW/m² occurs over a lateral distance of just a few kilometers, requiring the depth to the top of the hydrothermally active layer to be only a few hundred meters into basement.

It thus appears that most of the EPR-generated seafloor in the TicoFlux area is cooled by hydrothermal fluids and that basaltic outcrops facilitate the recharge and discharge of these fluids. *Langseth and Silver* [1996] argued that vigorous hydrothermal circulation was likely responsible for extreme cooling of the oceanic crust around ODP Site 1039, and *Silver et al.* [2001] used the observed extent of cooling to estimate a range of possible fluid-flow rates, driving forces, and crustal permeabilities. The basis for these calculations was the well-mixed aquifer model [*Langseth and Herman*, 1981], which is a one-dimensional representation of rapid lateral fluid flow superimposed on efficient local mixing in upper basement. We refine the results of earlier calculations [*Silver et al.*, 2001] on the basis of new data collected during the TicoFlux program.

Perdido outcrop is the closest seafloor basement exposure to ODP Site 1039 (fig. 4.1) and thus the most likely source of recharging hydrothermal fluid in this area. The upper oceanic crust is broken, uplifted, and exposed on the southwest side of the fracture zone [*Barckhausen et al.*, 2001], and heat-flow measurements made on the northwest side of this feature included the lowest values measured in the area ($<4\text{--}9\text{ mW/m}^2$). These low heat-flow values extend 3–10 km from the point of basement exposure, helping to place a strong constraint on the rate of lateral fluid flow within basement.

Assuming a typical sediment thickness of 500 m (as seen in seismic lines across the fracture zone), lateral fluid flow having a specific discharge (rate of discharge per unit area) of 3–30 m/yr within the upper 100–600 m of basement is required to suppress heat flow by 90–96% at a distance of 3–10 km from the recharge point (fig. 4.15a).

Thermal data from the cool part of the EPR-generated plate indicate upper-basement temperatures on the order of 20°C. As mentioned earlier, the primary driving force for ridge-flank hydrothermal circulation is the difference in pressure at the base of recharging and discharging water columns. We can calculate the greatest possible driving force for ridge-flank circulation by assuming that fluid recharge and discharge are adiabatic and that no energy is lost during fluid descent or ascent through the crust [e.g., *Fisher and Becker*, 2000]. The difference in pressures at the base of columns of recharging and discharging hydrothermal fluid is 20–50 kPa, assuming penetration to basement depths of 100–1000 m (fig. 4.15b). Finally, we can see from newly acquired swath-map data that the nearest exit points for hydrothermal fluids are outcrops located 75–110 km from Perdido seamount (fig. 4.1). As mentioned earlier, heat-flow data collected across normal faults on the seaward side of the trench give no evidence for fluid discharge (fig. 4.9) nor did an outcrop exposed near the trench in this area [*Fisher et al.*, 2003b].

Given a lateral specific discharge of 3–30 m/yr and a driving force of 20–50 kPa, upper-basement permeability in this area must be no less than 10^{-10} m^2 and could be as great as 10^{-8} m^2 (fig. 4.15b). These values at first seem surprisingly high for 18–24 Ma seafloor, but they are comparable to observations in other settings and earlier global predictions. Crustal permeabilities of 10^{-13} to 10^{-11} m^2 were estimated on the basis of single-hole packer and free-flow experi-

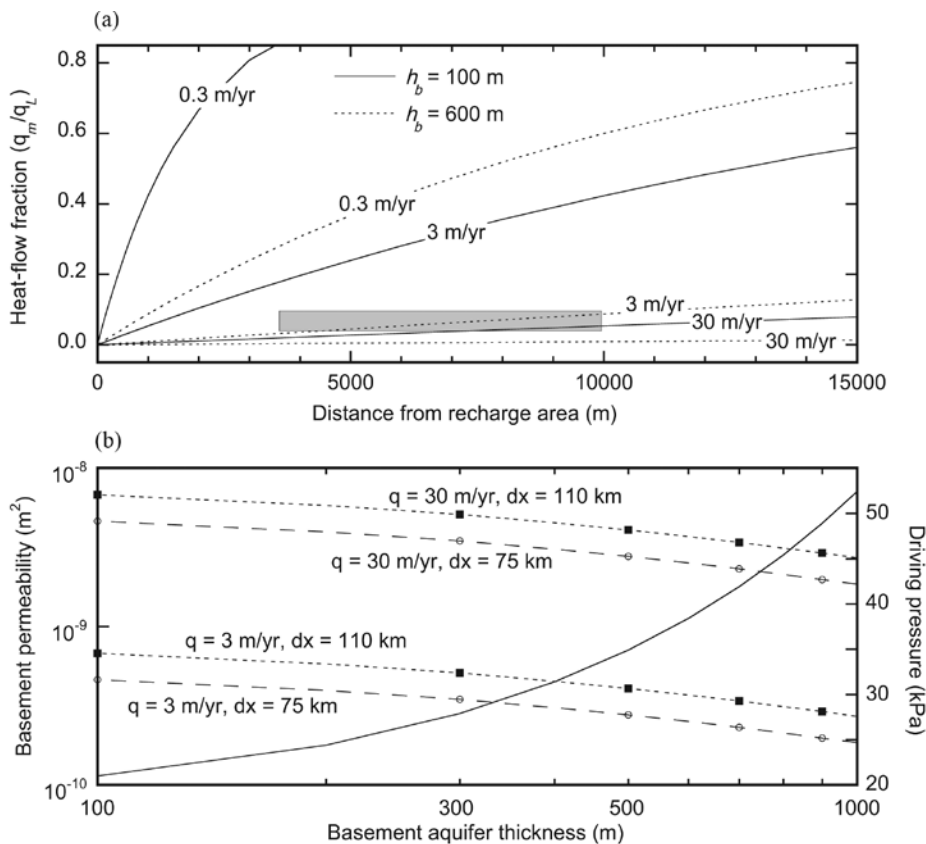


Figure 4.15 Calculations of fluid-flow rates, driving forces, and basement permeabilities required by TicoFlux data. (a) Results of well-mixed aquifer calculations [Langseth and Herman, 1981]. Specific discharge values are as indicated, h_b is the thickness of basement aquifer below 500 m of sediments. Heat-flow fraction is the ratio of measured to lithospheric heat-flow values. Gray box represents observations near Perdido outcrop, where measured heat flow is suppressed by 90–96% at a distance of 3–10 km from the outcrop. (b) Calculations of driving forces (solid line) and bulk basement permeabilities (dashed lines), based on consideration of fluid density differences between recharging and discharging outcrops (methods described in text and in greater detail by Fisher and Becker [2000] and Fisher et al. [2003a]). The temperature of fluids in upper basement was assumed to be 20°C, consistent with observations on the cool part of EPR-generated crust in this area. Outcrop spacing was constrained to be at least 75–110 km, based on available satellite-derived and swath maps. If the actual spacing between recharge and discharge sites is greater, bulk permeability in upper basement must be higher than shown.

ments within 3.5 Ma seafloor on the eastern flank of the Juan de Fuca Ridge, but higher permeabilities were estimated on the basis of crustal-scale flow and tidal analyses [e.g., Becker and Davis, 2003; Becker and Fisher, 2000; Davis et al., 2000; Fisher et al., 1997; Fisher et al., 2003a]. In a study of global heat flow and

permeability patterns, it was suggested that crustal-scale permeabilities of 10^{-8} to 10^{-10} m² are required by thermal observations on 20 Ma seafloor [Fisher and Becker, 2000]. Estimated driving forces and flow rates, and thus apparent basement permeabilities, scale roughly linearly with assumed depths of fluid penetration. Unfortunately, there are no observations from the TicoFlux surveys that help to constrain the depth extent of the large-scale lateral flow system responsible for very low heat-flow values common on EPR-generated seafloor in this area. However, data collected in other ridge-flank settings suggest that the uppermost few hundred meters are likely to be the most permeable [e.g., Alt et al., 1986; Bartzeko et al., 2001; Fisher, 1998].

The 3–30 m/yr specific discharge values calculated for the TicoFlux area are similar to flow rates inferred between widely spaced outcrops on the 3.5 Ma Juan de Fuca eastern flank [Fisher et al., 2003a]. Unlike conditions within most EPR-generated seafloor in the TicoFlux area, there is no regional heat-flow deficit between the Juan de Fuca flank outcrops. However, rapid fluid flow in that area appears to be largely restricted to the region between the outcrops. In contrast, extraction of heat from most of the EPR-generated seafloor along the MAT in the TicoFlux area requires that much of the crust in this area host vigorous fluid circulation.

Within the region of generally cool, EPR-generated seafloor, there are several relatively small areas of elevated heat flow (figs. 4.1 and 4.10). These are likely to result from heterogeneities in the distribution of basement permeability; either “stagnant” zones in which no fluid circulation occurs or regions where vigorous local fluid circulation is hydrologically isolated from the regional flow system. It should not be surprising that such regions exist, because fractured hydrogeologic systems tend to be heterogeneous on a range of scales [e.g., Fisher, 1998; Neuman, 1994; Neuman and Di Federico, 2003]. In addition, we found small areas on CNS-generated seafloor with anomalously low heat flow, and none of these are located immediately southeast of the fracture zone and adjacent to the MAT, where there are no basement outcrops penetrating through the seafloor. Even closer to the Cocos Ridge, where we measured a few low heat-flow values, these are associated with localized circulation; there is no evidence for large-scale, lateral fluid flow systems on CNS-generated seafloor in this area.

There are several possible explanations for the difference in thermal state across the two regions of the Cocos plate surveyed during the TicoFlux expeditions. First, there may be a difference in overall crustal permeability between warm and cool sides of the plate. Second, there could be one or more hydrogeologic boundaries within crust that otherwise has similar properties. Finally, it may be that the density and proximity of seamounts and other basement outcrops limit the lateral extent of penetration of cool, rapidly flowing fluids.

If the first or second explanations were correct, we might expect that the thermal transition across the Cocos plate would coincide with one or more of the major tectonic boundaries. Instead, the thermal transition coincides with

the plate suture (fracture zone trace) only where the plate is very close to the MAT (fig. 4.1). It is possible that there are one or more smaller-scale tectonic features associated with the part of the thermal transition that is offset from the plate suture but that such features are too small to be imaged clearly with the available seismic data. Subvertical fault offsets in basement of 20 m or less would likely be below the resolution of our instrumentation.

Another possible explanation for the lack of tectonic features associated with the thermal transitions is that seismic layer 2A (generally thought to be the most permeable part of oceanic basement on ridge flanks) is masked by sills, which are common in both the low and high heat-flow regions [*Silver et al.*, 2004]. The presence of sills could prevent seismic identification of faults in upper basement.

It is striking that, where the Cocos plate thermal transition is offset by 30–40 km from the plate suture, it runs close to a series of seamounts and other basement outcrops. It may be that there is no fundamental discontinuity in structure or hydrogeologic properties associated with the thermal transition in this area, but that the lack of outcrops on the warm side of the plate prevents significant advective heat extraction from basement. If this explanation is correct, there may be a critical combination of basement hydrogeologic properties and outcrop density that allows for the observed hydrothermal patterns. Moreover, there may be unusually high basement permeability within EPR-generated seafloor in this area, such that highly efficient advective heat extraction results from the imposition of closely spaced basaltic outcrops [e.g., *Fisher et al.*, 2003b]. We will explore these concepts in future studies using two- and three-dimensional numerical models.

Finally, we note that low heat flow on EPR-generated seafloor in this area occurs well seaward of the MAT, long before there is creation or reactivation of normal faults near the trench. The average heat flow of the incoming crust is the same as crust of its age far away from subduction zones [*Stein*, 2003]. There may be additional cooling in the trench associated with faulting and other subduction-related deformation [*Kimura et al.*, 1997; *Langseth and Silver*, 1996], but hydrothermal fluids extract an average of ~70% of lithospheric heat from most EPR-generated seafloor well before the plate reaches the trench. Thus vigorous fluid circulation must result from fundamental crustal construction and modification processes and is not directly related to subduction.

Implications of Hydrothermal Circulation and Thermal State of the Oceanic Crust on Subduction

One of the primary factors influencing the thermal regime of a subduction zone is the thermal state of the incoming oceanic plate as it enters the trench. The ability of hydrothermal circulation to redistribute heat and cool the incom-

ing oceanic crust, as well as chemically bind additional water in the form of mineralogical and rheological transformations (i.e., peridotite to serpentinite), may have an important influence on the updip limit of the seismogenic zone. The extent to which hydrothermal cooling influences subduction processes depends, in part, on the depth extent of fluid circulation and heat extraction.

Unfortunately, new data collected during the TicoFlux expeditions do not provide a robust constraint on the depth extent of circulation. Numerical and analytical models require that the top of the hydrothermally active basement is no more than 100–600 m below the sediments and allow observational constraints to be satisfied with flow restricted to the upper 600 m of basement.

If high-angle normal faults associated with plate flexure penetrate to several kilometers, it is possible that circulating fluids cool the plate to similar or greater depths. Any additional heat generated by serpentinization due to the influx of seawater along bend-related normal faults outboard of the MAT must also be extracted advectively, since heat flow within the trench is only ~10% of lithospheric.

We note that the ODP Leg 170 drilling transect is surrounded on three sides by regions of elevated heat flow (fig. 4.1). Temperature of upper basement at Site 1039 on the incoming plate is ~6°C [Kimura *et al.*, 1997], whereas upper-basement temperatures ~40 km to the south near Perdido outcrop and ~50 km to the west at station TF1-HF04,11 (fig. 4.10) are ~50°C. Warm and cool subduction zones have been shown to exhibit differences in seismicity [Peacock and Wang, 1999], reflecting the differences in metamorphic reactions occurring within the subducted crust. The along-strike variability of ~50°C in upper-basement temperature surrounding the ODP Leg 170 transect will have an impact on the thermal structure of the subduction thrust. If hydrothermal circulation is restricted to uppermost basement, its thermal influence on subduction will be limited. Assuming efficient hydrothermal cooling to a depth of 1 km into basement, two-dimensional thermal models of subduction suggest that thermal rebound will occur by the time the plate has moved ~50 km landward of the trench axis (see fig. 4.3, Harris and Wang [2002] and fig. 4.2, Spinelli and Saffer [2004]), which may influence the updip limit of seismicity [Hyndman *et al.*, 1997; Hyndman and Wang, 1993; Oleskevich *et al.*, 1999]. Studies of the seismogenic zone in this region show a shallowing of the updip limit in seismicity toward the south [Newman *et al.*, 2002] consistent with warmer basement temperatures.

Conclusions

Early studies on the Costa Rica margin identified areas of higher (>100 mW/m²) and lower (<30 mW/m²) heat flow on CNS- and EPR-generated seafloor, respectively. However, the sparse distribution of early heat flow, seismic, and

bathymetric data precluded confident determination of the causes of the heat-flow deficit on EPR-generated crust. In addition, there were no heat-flow measurements close to regional tectonic boundaries or basement exposures, making it impossible to determine if the thermal transition between anomalously cool and warm seafloor was associated with any of these features.

On the basis of newly acquired hydrosweep coverage, we find that seamounts with a characteristic spacing of 10–40 km are common features on EPR-generated seafloor north of the plate suture, whereas CNS-generated seafloor immediately adjacent to the plate suture and MAT appears to be entirely devoid of seamounts. These outcrops provide permeable pathways for the advective exchange of fluids and heat between the crust and overlying ocean, allowing hydrothermal fluids to bypass low-permeability sediments and efficiently extract large amounts of lithospheric heat. Most of the EPR-generated crust in the TicoFlux study region is cooled by rapidly flowing hydrothermal fluids, but we find no evidence for large-scale advective heat extraction in CNS-generated seafloor. Using observational data in the vicinity of Perdido outcrop as model constraints, lateral fluid flow having a specific discharge of 3–30 m/yr within the upper 100–600 m of basement can suppress heat flow by over 90% at a distance of 3–10 km from the recharge point. This requires that basement permeability in the area be on the order of 10^{-10} to 10^{-8} m². Although these values may seem high for this age of seafloor, they are comparable to estimates from other settings and are consistent with earlier global predictions.

We find purely conductive thermal conditions on one crossing of the ridge jump, and one crossing of the plate suture demonstrates vigorous hydrothermal circulation within uppermost basement. We find no thermal evidence for upward expulsion of fluids along bend-related normal faults outboard of the MAT near ODP Site 1039. There are areas on both EPR- and CNS-generated seafloor where rapid hydrothermal circulation associated with buried basement highs homogenizes upper-basement temperatures. Because the entire region of low heat flow on EPR-generated crust developed well seaward of the MAT, vigorous fluid circulation must result from fundamental crustal construction and modification processes and is not directly related to subduction.

The lack of a clear association between much of the interplate thermal transition with major tectonic boundaries suggests that other factors control fluid and heat flow in basement. If variations in crustal permeability or hydrogeologic boundaries were guiding or limiting flow, then we would expect the thermal transition between warm and cool parts of the Cocos plate to coincide with one or more tectonic boundaries (some of which may be seismically unresolvable). Where the thermal transition on EPR-generated seafloor is offset by 30–40 km from the plate suture, it runs alongside a series of seamounts and exposed basement outcrops that are actively recharging and discharging hydrothermal fluids between the crustal aquifer and the overlying ocean. This advective exchange of fluid and heat may be sufficient to create the observed

thermal patterns, without the requirement for fundamental discontinuities in structural or hydrogeologic properties.

Acknowledgments

We thank the officers, crew, and technicians of the R/V *Maurice Ewing* and R/V *Melville* for their assistance and advice during the TicoFlux expeditions. Data from the R/V *Meteor* M54-2 cruise were generously provided by Ingo Grevemeyer. C. Ranero provided a compilation of earlier bathymetric data. SeisWorks and Promax software were provided by a grant from Landmark Graphics Corporation. This work was supported by NSF grants OCE-0001892 (A.F. and E.S.), OCE-0001944 (R.H.), and OCE-0001941 (C.S.), and IGPP/LANL grant 1317 (A.F.). This research used samples and/or data provided by the Ocean Drilling Program (ODP). The ODP is sponsored by the U.S. National Science Foundation (NSF) and participating countries under management of Joint Oceanographic Institutions (JOI), Inc. Funding for this research was provided by a Schlanger Ocean Drilling Fellowship, which is sponsored by the NSF-funded U.S. Science Support Program (USSSP).

References

- Alt, J. C., J. Honnorez, C. Laverne, and R. Emmermann (1986), Hydrothermal alteration of a 1-km section through the upper oceanic crust, Deep Sea Drilling Project Hole 504B: Mineralogy, chemistry and evolution of seawater-basalt interactions, *J. Geophys. Res.*, *91*, 10,309–10,335.
- Alt, J. C., D. A. H. Teagle, C. Laverne, D. A. Vanko, W. Bach, J. Honnorez, K. Becker, M. Ayadi, and P. A. Pezard (1996), Ridge-flank alteration of upper oceanic crust in the eastern Pacific: Synthesis of results for volcanic rocks of Holes 504B and 896A, *Proc. Ocean Drill. Program Sci. Results*, *148*, 435–450.
- Anderson, R., and M. Hobart (1976), The relation between heat flow, sediment thickness, and age in the eastern Pacific, *J. Geophys. Res.*, *81*, 2968–2989.
- Barckhausen, U., C. Renaro, R. von Huene, S. C. Cande, and H. A. Roeser (2001), Revised tectonic boundaries in the Cocos Plate off Costa Rica: Implications for the segmentation of the convergent margin and for plate tectonic models, *J. Geophys. Res.*, *106*, 19,207–19,220.
- Bartetzko, A., P. Pezard, D. Goldberg, Y.-F. Sun, and K. Becker (2001), Volcanic stratigraphy of DSDP/ODP Hole 395A: An interpretation using well-logging data, *Mar. Geophys. Res.*, *22*, 111–127.
- Becker, K., and E. Davis (2003), New evidence for age variation and scale effects of permeabilities of young oceanic crust from borehole thermal and pressure measurements, *Earth Planet. Sci. Lett.*, *210*, 499–508.
- Becker, K., and A. Fisher (2000), Permeability of upper oceanic basement on the eastern flank of the Endeavor Ridge determined with drill-string packer experiments, *J. Geophys. Res.*, *105*, 897–912.
- Becker, K., M. Langseth, R. P. Von Herzen, and R. Anderson (1983), Deep crustal geothermal measurements, Hole 504B, Costa Rica Rift, *J. Geophys. Res.*, *88*, 3447–3457.

- Bevington, P. R., and D. K. Robinson (1992), *Data Reduction and Error Analysis for the Physical Sciences*, 328 pp., McGraw-Hill, New York.
- Bredehoeft, J. D., and I. S. Papadopoulos (1965), Rates of vertical groundwater movement estimated from the Earth's thermal profile, *Water Resour. Res.*, *1*, 325–328.
- Bullard, E. C., A. E. Maxwell, and R. Revelle (1956), Heat flow through the deep sea floor, *Adv. Geophys.*, *3*, 153–181.
- Busch, W. H., P. R. Castillo, P. A. Floyd, and G. Cameron (1992), Effects of alteration on physical properties of basalts from the Pigafetta and East Mariana basins, *Proc. Ocean Drill. Program Sci. Results* *129*, 485–500.
- Carlson, R. L. (1998), Seismic velocities in the uppermost oceanic crust: Age dependence and the fate of layer 2A, *J. Geophys. Res.*, *103*, 7069–7077.
- Cowen, J. P., S. J. Giovannoni, F. Kenig, H. P. Johnson, D. Butterfield, M. S. Rappé, M. Hutnak, and P. Lam (2003), Fluids from aging ocean crust that support microbial life, *Science*, *299*, 120–123.
- Davis, E. E., and K. Becker (2002), Observations of natural-state fluid pressures and temperatures in young oceanic crust and inferences regarding hydrothermal circulation, *Earth Planet. Sci. Lett.*, *204*, 231–248.
- Davis, E. E., D. S. Chapman, C. Forster, and H. Villinger (1989), Heat-flow variations correlated with buried basement topography on the Juan de Fuca Ridge flank, *Nature*, *342*, 533–537.
- Davis, E. E., et al. (1992), FlankFlux: An experiment to study the nature of hydrothermal circulation in young oceanic crust, *Can. J. Earth Sci.*, *29*(5), 925–952.
- Davis, E. E., D. S. Chapman, K. Wang, H. Villinger, A. T. Fisher, S. W. Robinson, J. Grigel, D. Pribnow, J. Stein, and K. Becker (1999), Regional heat-flow variations across the sedimented Juan de Fuca Ridge eastern flank: Constraints on lithospheric cooling and lateral hydrothermal heat transport, *J. Geophys. Res.*, *104*, 17,675–17,688.
- Davis, E. E., K. Wang, K. Becker, and R. E. Thomson (2000), Formation-scale hydraulic and mechanical properties of oceanic crust inferred from pore-pressure response to periodic seafloor loading, *J. Geophys. Res.*, *105*, 13,423–13,435.
- DeMets, C. (2001), A new estimate for present-day Cocos-Caribbean plate motion: Implications for slip along the Central American volcanic arc, *Geophys. Res. Lett.*, *28*, 4043–4046.
- Elder, J. W. (1965), Physical processes in geothermal areas, in *Terrestrial Heat Flow*, *Geophys. Monogr. Ser.*, vol. 8, edited by W. H. K. Lee, pp. 211–239, AGU, Washington, D. C.
- Elderfield, H., and A. Schultz (1996), Mid-ocean ridge hydrothermal fluxes and the chemical composition of the ocean, *Annu. Rev. Earth Planet. Sci.*, *24*, 191–224.
- Elderfield, H., C. G. Wheat, M. J. Mottl, C. Monnin, and B. Spiro (1999), Fluid and geochemical transport through oceanic crust: A transect across the eastern flank of the Juan de Fuca Ridge, *Earth Planet. Sci. Lett.*, *172*, 151–165.
- Fisher, A. (2004), Rates and patterns of fluid circulation, in *Hydrogeology of the Oceanic Lithosphere*, edited by E. E. Davis and H. Elderfield, pp. 339–377, Cambridge Univ. Press, New York.
- Fisher, A. T. (1998), Permeability within basaltic oceanic crust, *Rev. Geophys.*, *36*, 143–182.
- Fisher, A. T., and K. Becker (2000), Channelized fluid flow in oceanic crust reconciles heat-flow and permeability data, *Nature*, *403*, 71–74.
- Fisher, A. T., K. Becker, T. N. Narasimhan, M. G. Langseth, and M. J. Mottl (1990), Passive, off-axis convection on the southern flank of the Costa Rica Rift, *J. Geophys. Res.*, *95*, 9343–9370.
- Fisher, A. T., K. Becker, and E. E. Davis (1997), The permeability of young oceanic crust east of Juan de Fuca Ridge determined using borehole thermal measurements, *Geophys. Res. Lett.*, *24*, 1311–1314.
- Fisher, A. T., et al. (2003a), Hydrothermal recharge and discharge across 50 km guided by seamounts on a young ridge flank, *Nature*, *421*, 618–621.

- Fisher, A. T., C. A. Stein, R. N. Harris, K. Wang, E. A. Silver, M. Pfender, M. Hutnak, A. Cherkouki, R. Bodzin, and H. Villinger (2003b), Abrupt thermal transition reveals hydrothermal boundary and role of seamounts within the Cocos Plate, *Geophys. Res. Lett.*, 30(11), 1550, doi:10.1029/2002GL016766.
- Gaetani, G. A., and T. L. Grove (1998), The influence of water on mantle melting, *Contrib. Mineral. Petrol.*, 131, 323–346.
- Giambalvo, E., A. T. Fisher, L. Darty, J. T. Martin, and R. P. Lowell (2000), Origin of elevated sediment permeability in a hydrothermal seepage zone, eastern flank of Juan de Fuca Ridge, and implications for transport of fluid and heat, *J. Geophys. Res.*, 105, 913–928.
- Harris, R. N., and K. Wang (2002), Thermal models of the Middle America Trench at the Nicoya Peninsula, Costa Rica, *Geophys. Res. Lett.*, 29(21), 2010, doi:10.1029/2002GL015406.
- Henry, P., and C.-Y. Wang (1991), Modeling of fluid flow and pore pressure at the tow of the Barbados and Oregon accretionary wedges, *J. Geophys. Res.*, 96, 20,109–20,130.
- Hey, R. N. (1977), Tectonic evolution of the Cocos-Nazca spreading center, *Geol. Soc. Am. Bull.*, 88, 1404–1420.
- Hyndman, R., M. Yamano, and D. Oleskevich (1997), The seismogenic zone of subduction thrust faults, *Island Arc*, 6(3), 244–260.
- Hyndman, R. D., and K. Wang (1993), Thermal constraints on the seismogenic portion of the southwestern Japan subduction zone of subduction thrust faults, *J. Geophys. Res.*, 100, 2039–2060.
- Hyndman, R. D., E. E. Davis, and J. A. Wright (1979), The measurement of marine geothermal heat flow by a multipenetration probe with digital acoustic telemetry and in situ conductivity, *Mar. Geophys. Res.*, 4, 181–205.
- Iwamori, H. (1998), Transportation of H₂O and melting in subduction zones, *Earth Planet. Sci. Lett.*, 60, 65–80.
- Jacobson, R. S. (1992), Impact of crustal evolution on changes of the seismic properties of the uppermost oceanic crust, *Rev. Geophys.*, 30, 23–42.
- Johnson, H. P., K. Becker, and R. P. V. Herzen (1993), Near-axis heat flow measurements on the northern Juan de Fuca Ridge: Implications for fluid circulation in oceanic crust, *Geophys. Res. Lett.*, 20, 1875–1878.
- Karato, S. (1983), Physical properties of basalts from Deep Sea Drilling Project Hole 504B, *Initial Rep. Deep Sea Drill. Proj.*, 69, 687–695.
- Kelley, D. S., et al. (2001), An off-axis hydrothermal vent field near the Mid-Atlantic Ridge at 30°N, *Nature*, 412, 145–149.
- Kimura, G., E. Silver, and P. Blum (1997), *Proceedings of the Ocean Drilling Program, Initial Reports*, 458 pp., Ocean Drill. Program, College Station, Tex.
- Langseth, M. G., and B. Herman (1981), Heat transfer in the oceanic crust of the Brazil Basin, *J. Geophys. Res.*, 86, 10,805–10,819.
- Langseth, M. G., and E. A. Silver (1996), The Nicoya convergent margin - A region of exceptionally low heat flow, *Geophys. Res. Lett.*, 23, 891–894.
- Langseth, M. G., P. J. Grim, and M. Ewing (1965), Heat-flow measurements in the east Pacific Ocean, *J. Geophys. Res.*, 70, 367–380.
- Langseth, M. G., X. LePichon, and M. Ewing (1966), Crustal structure of the midocean ridges, 5, heat flow through the Atlantic Ocean floor and convection currents, *J. Geophys. Res.*, 71, 5321–5355.
- Langseth, M. G., M. J. Mottl, M. A. Hobart, and A. T. Fisher (1988), The distribution of geothermal and geochemical gradients near Site 501/504, implications for hydrothermal circulation in the oceanic crust, in *Proc. Ocean Drill. Program Initial Rep.*, 111, 23–32.
- Lee, W. H. K., and S. Uyeda (1965), Review of heat flow data, in *Terrestrial Heat Flow, Geophys. Monogr. Ser.*, vol. 8, edited by W. H. K. Lee, pp. 87–190, AGU, Washington, D. C.
- Lowell, R. P. (1980), Topographically driven subcritical hydrothermal convection in the oceanic crust, *Earth Planet. Sci. Lett.*, 49, 21–28.

- Lowell, R. P., and P. A. Rona (2002), Seafloor hydrothermal systems driven by the serpentinization of peridotite, *Geophys. Res. Lett.*, *29*(11), 1531, doi:10.1029/2001GL014411.
- McIntosh, K., and M. Sen (2000), Geophysical evidence for dewatering and deformation processes in the ODP Leg 170 area offshore Costa Rica, *Earth Planet. Sci. Lett.*, *178*, 125–138.
- Meschede, M., U. Barckhausen, and H.-U. Worm (1998), Extinct spreading on the Cocos Ridge, *Terra Nova*, *10*, 211–216.
- Mottl, M. J., and C. G. Wheat (1994), Hydrothermal circulation through mid-ocean ridge flanks: Fluxes of heat and magnesium, *Geochim. Cosmochim. Acta*, *58*, 2225–2237.
- Neuman, S. P. (1994), Generalized scaling of permeabilities: Validation and effect of support scale, *Geophys. Res. Lett.*, *21*, 349–352.
- Neuman, S. P., and V. Di Federico (2003), Multifaceted nature of hydrogeologic scaling and its interpretation, *Rev. Geophys.*, *41*(3), 1014, doi:10.1029/2003RG000130.
- Newman, A. V., S. Y. Schwartz, H. R. DeShon, J. M. Protti, V. Gonzalez, and L. Dorman (2002), Along-strike variability in the seismogenic zone below Nicoya Peninsula, Costa Rica, *Geophys. Res. Lett.*, *29*(20), 1977, doi:10.1029/2002GL015409.
- Noel, M., and M. W. Hounslow (1988), Heat flow evidence for hydrothermal convection in Cretaceous crust of the Madeira Abyssal Plain, *Earth Planet. Sci. Lett.*, *90*, 77–86.
- Oleskevich, D., R. Hyndman, and K. Wang (1999), The updip and downdip limits to great subduction earthquakes: Thermal and structural models of Cascadia, south Alaska, SW Japan, and Chile, *J. Geophys. Res.*, *104*, 14,965–14,991.
- Parsons, B., and J. G. Sclater (1977), An analysis of the variation of ocean floor bathymetry and heat flow with age, *J. Geophys. Res.*, *82*, 803–829.
- Peacock, S. M. (2001), Are the lower planes of double seismic zones caused by serpentine dehydration in subducting oceanic mantle, *Geology*, *29*, 299–302.
- Peacock, S. M., and K. Wang (1999), Seismic consequences of warm versus cool subduction metamorphism: Examples for southwest and northeast Japan, *Science*, *286*, 937–939.
- Pfender, M., and H. Villinger (2002), Miniaturized data loggers for deep sea sediment temperature gradient measurements, *Mar. Geol.*, *186*(3–4), 557–570.
- Plank, T., and C. H. Langmuir (1993), Tracing trace elements from sediment input to volcanic output at subduction zones, *Nature*, *362*, 739–742.
- Ranero, C. R., and R. von Huene (2000), Subduction erosion along the Middle America convergent margin, *Nature*, *404*, 748–752.
- Ranero, C. R., J. Phipps Morgan, and R. von Huene (2003), Bending-related faulting and mantle serpentinization at the Middle America Trench, *Nature*, *405*, 367–373.
- Rohr, K. (1994), Increase of seismic velocities in upper oceanic crust and hydrothermal circulation in the Juan de Fuca plate, *Geophys. Res. Lett.*, *21*, 2163–2166.
- Ruppel, C., and M. Kinoshita (2000), Fluid, methane, and energy flux in an active margin gas hydrate province, offshore Costa Rica, *Earth Planet. Sci. Lett.*, *179*, 153–165.
- Saffer, D., and C. Marone (2003), Comparison of smectite- and illite-rich gouge frictional properties: Application to the updip limit of the seismogenic zone along subduction megathrusts, *Earth Planet. Sci. Lett.*, *215*, 219–235.
- Schultz, A., and H. Elderfield (1997), Controls on the physics and chemistry of seafloor hydrothermal circulation, *Philos. Trans. R. Soc. London, Ser. A*, *355*(1723), 387–425.
- Sclater, J. G., J. Crowe, and R. Anderson (1976), On the reliability of oceanic heat flow averages, *J. Geophys. Res.*, *81*, 2997–3006.
- Sclater, J. G., C. Jaupart, and D. Galson (1980), The heat flow through oceanic and continental crust and the heat loss of the earth, *Rev. Geophys.*, *18*, 269–311.
- Silver, E., M. Kastner, A. Fisher, J. Morris, K. McIntosh, and D. Saffer (2001), Fluid flow paths in the crust of the Middle America Trench, Costa Rica margin, *Geology*, *28*(8), 679–682.
- Silver, E., P. C. Pisani, M. Hutnak, A. Fisher, H. R. DeShon, and B. Taylor (2004), An 8–10 Ma tectonic event on the Cocos Plate offshore Costa Rica: Result of Cocos Ridge collision?, *Geophys. Res. Lett.*, *31*, L18601, doi:10.1029/2004GL020272.

- Smith, W. H. F., and D. T. Sandwell (1997), Global sea floor topography from satellite altimetry and ship depth soundings, *Science*, 277, 1956–1962.
- Spinelli, G. A., and D. Saffer (2004), Along-strike variations in underthrust sediment dewatering on the Nicoya margin, Costa Rica related to the updip limit of seismicity, *Geophys. Res. Lett.*, 31, L04613, doi:10.1029/2003GL018863.
- Stein, C. (2003), Heat flow and flexure at subduction zones, *Geophys. Res. Lett.*, 30(23), 2197, doi:10.1029/2003GL018478.
- Stein, C., and S. Stein (1992), A model for the global variation in oceanic depth and heat flow with lithospheric age, *Nature*, 359, 123–129.
- Stein, C., and S. Stein (1994), Constraints on hydrothermal heat flux through the oceanic lithosphere from global heat flow, *J. Geophys. Res.*, 99, 3081–3095.
- Stein, J. S., and A. T. Fisher (2001), Multiple scales of hydrothermal circulation in Middle Valley, northern Juan de Fuca Ridge: Physical constraints and geologic models, *J. Geophys. Res.*, 106, 8563–8580.
- Vacquier, V., J. G. Sclater, and C. E. Corry (1967), Studies in the thermal state of the earth, the 21st paper: Heat-flow, Eastern Pacific, *Bull. Earthquake Res. Inst.*, 45, 375–393.
- Villinger, H., and E. E. Davis (1987), HFRED: A program for reduction of marine heat flow data on a microcomputer, report, 77 pp., Geol. Surv. of Can., Sydney, B. C.
- Villinger, H., I. Grevemeyer, N. Kaul, J. Hauschild, and M. Pfender (2002), Hydrothermal heat flux through aged oceanic crust: Where does the heat escape?, *Earth Planet. Sci. Lett.*, 202(1), 159–170.
- Von Herzen, R., and S. Uyeda (1963), Heat flow through the eastern Pacific floor, *J. Geophys. Res.*, 68, 4219–4250.
- Von Herzen, R. P. (2004), Geothermal evidence for continuing hydrothermal circulation in older (>60 Ma) ocean crust, in *Hydrogeology of the Oceanic Lithosphere*, edited by E. E. Davis and H. Elderfield, pp. 414–450, Cambridge Univ. Press, New York.
- von Huene, R., C. R. Ranero, W. Wienrebe, and K. Hinz (2000), Quarternary convergent margin tectonics of Costa Rica, segmentation of the Cocos Plate, and Central American volcanism, *Tectonics*, 19, 314–334.
- Wessel, P. (2001), Global distribution of seamounts inferred from gridded Geosat/ERS-1 altimetry, *J. Geophys. Res.*, 106, 19,431–19,442.
- Wheat, C. G., and M. J. Mottl (1994), Hydrothermal circulation, Juan de Fuca Ridge eastern flank: Factors controlling basement water composition, *J. Geophys. Res.*, 99, 3067–3080.
- Wheat, C. G., J. McManus, M. Mottl, and E. G. Giambalvo (2003), Oceanic phosphorus imbalance: Magnitude of the mid-ocean ridge flank hydrothermal sink, *Geophys. Res. Lett.*, 30(17), 1895, doi:10.1029/2003GL017318.
- Yamano, M., and S. Uyeda (1990), Heat flow studies in the Peru Trench subduction zone, *Proc. Ocean Drill. Program Sci. Results*, 112, 653–662.
- Zhao, D., Y. Xu, D. A. Wiens, L. Dorman, J. Hildebrand, and S. Webb (1997), Depth extent of the Lau back arc spreading center and its relation to subduction processes, *Science*, 278, 254–257.
- Zyvoloski, G. A., B. A. Robinson, Z. D. Dash, and L. L. Trease (1996), *Users Manual for the FEHMN Application*, Los Alamos Natl. Lab., Los Alamos, N. M.